Computers & Fluids 111 (2015) 18–32

Contents lists available at ScienceDirect

Computers & Fluids

journal homepage: www.elsevier.com/locate/compfluid

Accurate solution and approximations of the linearized BGK equation for steady Couette flow

Wei Li [a], Li-Shi Luo [a,b,*], Jie Shen [c,d]

[a] Department of Mathematics & Statistics, Old Dominion University, Norfolk, VA 23529, USA
[b] Computational Science Research Center, Beijing 10084, China
[c] Fujian Provincial Key Laboratory on Mathematical Modeling & High Performance Scientific Computing and School of Mathematical Sciences, Xiamen University, Xiamen, China
[d] Department of Mathematics, Purdue University, West Lafayette, IN 47907, USA

ARTICLE INFO

Article history:
Received 13 August 2014
Received in revised form 6 December 2014
Accepted 17 December 2014
Available online 7 January 2015

Keywords:
Linearized BGK equation
Integral equation
Steady Couette flow
Chebyshev expansion
Collocation method

ABSTRACT

We present an accurate and efficient high-order collocation method to solve the integral equation with a singular kernel derived from the linearized BGK equation in kinetic theory. In particular, we use a Chebyshev based collocation method to solve the integral equation with singular kernel for the steady Couette flow in a wide range of Knudsen numbers, *i.e.*, $0.003 \leqslant k \leqslant 10.0$. We compute the flow velocity $u(y,k)$, the stress $P_{xy}(k)$, and the half-channel total mass flow rate $Q(k)$. Our results are uniformly accurate to 11 significant digits or better, thus they can serve as benchmark data. We also construct approximations of the velocity, the slip velocity, and the total mass flow rate as functions of the Knudsen number k.

1. Introduction

In rarefied-gas dynamics (RGD) and kinetic theory, the solutions of the Boltzmann equation for some canonical flows, such as Couette flow, Poiseuille flow, and Kramers' problem, have been much studied for a long time (cf. reviews [1,2] and monographs [3–8] and references therein). In particular, the linearized Bhatnagar–Gross–Krook (BGK) equation has been used to study these flows [1–8]. The linearized BGK equation for the canonical flows can be recast in an integral equation of the second kind in one dimension (1D) for the macroscopic flow velocity. Along with the advance of computing, there has been a persistent and rigorous effort to obtain accurate solutions of the integral equations for the canonical flows in kinetic theory [9–25], because the accurate solutions of these flows can provide the insights about the mathematical properties of these flows, so allow one to construct models for engineering applications.

Although there have been significant advances made in the techniques for solving various integral equations [26–35], these well developed solution techniques have not been widely adopted by the RGD community. Most studies on numerical solutions of the integral equations for the classical flows rely on the Nyström method (cf., *e.g.*, the monograph by Atkinson [36]) or quadrature method, which directly discretizes the continuous problem into n intervals and replaces the integral with a representative weighted sum. There are at least two inherent difficulties which are commonly encountered in existing numerical solutions of the integral equations. First and foremost, the quadratures used to solve the integral equations are not suitable for the integral equations with singular kernels. And second, the singular integral kernels are often represented in terms of the Meijer G-function [37,38], which are very likely to suffer from catastrophic cancellation for large values of the argument, and will also be difficult to use in the asymptotic range [39,40]. These two major difficulties prevent one to obtain high-precision benchmark solutions of the integral equations efficiently. The existing methodologies often are of low order in terms of their accuracy, and they require to solve a large linear system and to use multiple-precision arithmetic in order to obtain high-precision solutions.

There have been constant attempts to obtain high-precision benchmark solutions of the linearized BGK equation for canonical flows [19–22,25]. For Kramers' problem, Loyalka and Tompson [22] use the Nyström method with Gauss–Kronrod quadrature to discretize the integral equation. With the largest quadrature order of 1312 and the precision of 60 digits, Loyalka and Tompson are able to obtain the flow velocity with an accuracy of about 7 digits. More recently, Yap and Sader [25] use the same technique to solve the linearized BGK equation with Gauss–Legendre quadrature for

* Corresponding author at: Department of Mathematics & Statistics, Old Dominion University, Norfolk, VA 23529, USA.
E-mail addresses: lluo@odu.edu (L.-S. Luo), shen7@purdue.edu (J. Shen).

http://dx.doi.org/10.1016/j.compfluid.2014.12.018
0045-7930/

steady and oscillating Couette flows. With a precision of 30 digits, Yap and Sader achieve the rates of convergence greater than 3.0 and 1.0 on the order of quadrature N and the number of intervals L, respectively. The largest N and L are 160 and 80, respectively, resulting in a large linear system of the size $(160 \times 80)^2 = 12{,}800^2 = 163{,}840{,}000$. For the steady Couette flow, Yap and Sader obtain the velocity which is correct to 5, 7, and 8 significant digits for the Knudsen number $k = 0.01, k = 0.03$, and $k \geqslant 0.1$, respectively.

The intent of the present work is two fold. Our first intent is to implement an efficient high-order Chebyshev collocation method to solve the integral equation arisen from the linearized BGK equation. The singular kernel is to be given by its Chebyshev expansion [41]. This approach is both effective and efficient, thus overcomes the difficulty due to the Meijer G-function representation of the singular kernels. We will, in particular, solve the integral equation for steady Couette flow [1,9,10,15,20,25] with the Knudsen number k in a wide range of $0.003 \leqslant k \leqslant 10.0$. With mostly double-precision (64 bits) arithmetic, we can obtain the flow velocity and other interested quantities uniformly correct to 11 or more digits. Our results are significantly more accurate than existing ones, thus can be used as benchmark data. Our second intent is to construct approximated models based on the accurate solutions for various interested flow quantities, which can be used in engineering applications.

The remainder of the paper is organized as follows. Section 2 succinctly describes the integral equation for steady Couette flow and its solution technique based on Chebyshev collocation method. Section 3 presents our results. In Section 3.1 we demonstrate the convergence of our calculations to show that the collocation method is of high-order indeed. In Section 3.2 we present the benchmark data for the flow velocity, the shear stress, and the half-channel total mass flow rate in a wide range of the Knudsen number $0.003 \leqslant k \leqslant 10.0$, which covers flows regions from slip flow, transition flow, to free-molecular flow. In Section 3.3 we present approximated solutions for the flow velocity and analyze their validity and accuracy. And in Section 3.4 we analyze the velocity defect and slip velocity. Based on our analysis, we construct some approximations for slip velocity and the total mass flow rate which depends on the Knudsen layer structure. Finally, Section 4 concludes the paper. Three appendixes are supplemented for details. Appendix A provides a summary of the properties of and useful approximations for Abramowitz functions $I_n(x)$. Appendix B proves that the velocity derivative $u'(y,k)$ diverges at boundaries. And Appendix C provides the details of accurate evaluation of integrals involving Abramowitz function I_{-1} and Chebyshev polynomials T_n.

2. Integral equation for steady Couette flow and Chebyshev collocation method

We will study the integral equation derived from the linearized BGK equation [9,4,6] for the steady Couette flow between two parallel infinite horizontal plates, which move in opposite direction with the velocity $(\pm U/2, 0, 0)$, as shown in Fig. 1 for an illustration of the flow configuration. The flow is one-dimensional, *i.e.*, the flow fields are functions of the spanwise coordinate in $\hat{\boldsymbol{y}}$ direction, and invariant along the streamwise direction $\hat{\boldsymbol{x}}$, as illustrated in Fig. 1.

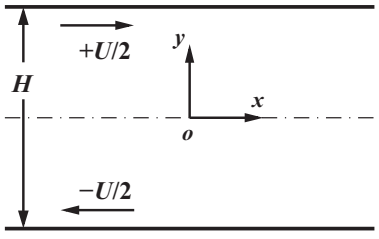

Fig. 1. An illustration of flow configuration of Couette flow.

For the steady Couette flow, the linearized BGK equation with the Maxwell boundary condition [42,5,8] leads to the following integral equation for the velocity $u(y,k)$ [9,6,8]:

$$u(y,k) - \frac{1}{k\sqrt{\pi}} \int_{-1/2}^{1/2} I_{-1}\left(\frac{|y-s|}{k}\right) u(s)\mathrm{d}s = \frac{1}{2\sqrt{\pi}} F_0(y,k), \tag{1a}$$

$$I_n(x) = \int_0^\infty s^n e^{-(s^2+x/s)}\mathrm{d}s, \quad n \geqslant -1, \tag{1b}$$

$$F_n(y,k) := \left[I_n\left(\frac{1-2y}{2k}\right) - I_n\left(\frac{1+2y}{2k}\right) \right], \tag{1c}$$

where y is normalized by the channel width H (cf. Fig. 1) so that $-1/2 \leqslant y \leqslant +1/2$, the velocity u is normalized by the relative wall speed U so that $-1/2 \leqslant u \leqslant +1/2, I_n(x)$ is the Abramowitz function of order $n, k = c_m/H\omega$ is the Knudsen number, $c_m := \sqrt{2RT_0}$, R is the gas constant, T_0 is a constant temperature, and ω is the constant relaxation frequency of the BGK equation [43].

Eq. (1a) is a Fredholm equation of the second kind with the kernel I_{-1}, the Abramowitz function of order -1, which has a logarithmic singularity at zero, which occurs at both end points $y = \pm 1/2$. (Some properties and approximations of Abramowitz function I_n relevant to this work are succinctly summarized in Appendix A.) The singular nature of the integral kernel I_{-1} makes it difficult to solve Eq. (1a) numerically. To mitigate the problem due to the end-point singularities, Eq. (1a) is rewritten as the following:

$$G_0(y,k)u(y) - \frac{1}{k} \int_{-1/2}^{1/2} I_{-1}\left(\frac{|y-s|}{k}\right) [u(s) - u(y)]\mathrm{d}s = \frac{1}{2} F_0(y,k), \tag{2a}$$

$$G_n(y,k) := \left[I_n\left(\frac{1-2y}{2k}\right) + I_n\left(\frac{1+2y}{2k}\right) \right]. \tag{2b}$$

It should be emphasized that while the term $[u(s) - u(y)]$ in the integral in Eq. (2a) is introduced to mitigate the difficulty caused by the end-point singularities, the singularities cannot be removed by this simple technique. Because the Knudsen number k appears in the denominator in the argument of $I_0(x)$ and $I_{-1}(x)$ in the integral equation of Eq. (1a) or (2a), it becomes more and more difficult to solve the equation when k becomes smaller and smaller. This is understandable because the thickness of the Knudsen layer becomes thinner as k decreases, thus it requires more and more resolution in a thinner and thinner layer in the vicinities about the singularities at the boundaries $y = \pm 1/2$.

It has been well known [9,44,45] that the leading order singularity in $u(y,k)$ at the end points $y = \pm 1/2$, is $\delta \ln \delta$, where $\delta := (1/2 \mp y)$ is the distance to the end-point $y = \pm 1/2$, as $\delta \to 0$. Only recently it has been shown [46] that $u(y,k)$ has singular terms of $(\delta \ln \delta)^m$, for all $m \geqslant 1$. The essential singularities at the boundaries present the main challenge to numerical solutions of the integral Eq. (1a).

We will use the collocation method with Chebyshev polynomials to solve the integral Eq. (2a). The velocity $u(y,k)$ is antisymmetric about the channel centerline $y = 0$, *i.e.*, $u(y) = -u(-y)$, because of the boundary conditions $u(\pm 1/2) = \pm 1/2$, thus it is expanded in terms of odd-order Chebyshev polynomial T_n with $n = (2j-1)$:

$$u_N(y) = \sum_{j=1}^{N} c_n T_n(2y), \quad n = 2j-1. \tag{3}$$

Then Eq. (2a) becomes a linear system for the coefficients $\{c_n | n = 2j-1,\ 1 \leqslant j \leqslant N\}$:

$$\sum_{j=1}^{N} c_n A_n(y) = \frac{1}{2} F_0(y,k), \tag{4a}$$

$$A_n(y) = G_0(y,k) T_n(2y) - \frac{1}{k}\int_{-1/2}^{1/2} I_{-1}\left(\frac{|y-s|}{k}\right)[T_n(2s) - T_n(2y)]\mathrm{d}s. \tag{4b}$$

Eq. (4a) can be solved either by a collocation method or a Galerkin method [36]. We choose a collocation method for its computational efficiency. With N collocation points $\{y_i | 1 \leqslant i \leqslant N\}$, we have a linear system for $\{c_n\}$

$$\mathsf{A} \cdot \mathbf{c} = \mathbf{b}, \quad \Rightarrow \quad \mathbf{c} = \mathsf{A}^{-1} \cdot \mathbf{b}, \tag{5}$$

where A is an $N \times N$ matrix whose element is $a_{mn} = A_n(y_m)$, and $\mathbf{b}$ and $\mathbf{c}$ are N-tuple column vectors whose elements are $b_m = F_0(y_m,k)/2$ and c_n, respectively, $m = (2i-1)$, $n = (2j-1)$, $1 \leqslant i, j \leqslant N$.

We use Gauss–Chebyshev collocation method with the following collocation points:

$$y_m = \frac{1}{2}\cos\theta_m, \quad \theta_m := \frac{(4m-1)\pi}{4N}, \quad 1 \leqslant m \leqslant N. \tag{6}$$

Note that the collocation points $\{y_m\}$ do not include end points $y = \pm 1/2$. With N collocation points $\{y_m | 1 \leqslant m \leqslant N\}$, we observe that the velocity $u_N(y)$ is accurate in the interval $(y_N - \epsilon, y_1 + \epsilon) \subset [-1/2, +1/2]$, where $\epsilon > 0$. That is, the numerics become less accurate near the vicinities of the end points $y = \pm 1/2$. In fact, the numerical accuracy of the quadrature in the interval $(1/2 - \epsilon, 1/2]$ is only about one half of that in the interior interval $(y_N - \epsilon, y_1 + \epsilon)$. To overcome this deficiency, we include one end point, say, $y = +1/2$, in the set of the collocation points. With this augmented set of collocation points, the quadrature is accurate in the vicinity of the included end point, *i.e.*, $(1/2 - \epsilon, 1/2]$. However, with the augmented set of collocation points the accuracy of the quadrature deteriorates in the interior $(y_N - \epsilon, y_1 + \epsilon)$. In fact, with the augmented set of collocation points the accuracy of the quadrature in the interior interval $(y_N - \epsilon, y_1 + \epsilon)$ is only about one half of the quadrature without the end point. Thus, to maintain a uniform accuracy in the entire interval $[-1/2, +1/2]$, we use the quadrature with the usual collocation points for $y \in [y_N, y_1]$, and the augmented set of collocation points with one end point, say $y = +1/2$, for the vicinity of the end point, say, $y \in [y_1, +1/2]$. More details about the numerics are given in Appendix C.

We intend to devise an effective and efficient numerical scheme to compute $u(y,k)$ with high precision. More specifically, we would like to obtain $u(y,k)$ with the accuracy of ten digits or better by using double-precision arithmetic. To attain this objective, we need to compute all the elements in linear system of Eq. (5) with desirable accuracy. First, we must accurately evaluate the zeroth-order Abramowitz function, I_0, which is accomplished by using the method of Chebyshev expansion proposed by MacLeod [41]. The approximations we use to evaluate the Abramowitz function are given in Appendix A.

The second part of the calculation is to accurately evaluate the integral in Eq. (4b). With high-order Chebyshev function $T_n(2y), n \gg 1$, the integrand in Eq. (4b) is highly oscillatory. Also, the integral is singular when the argument of I_{-1} is zero. To accurately evaluate the integral, we divide the interval $[-1/2, +1/2]$ into n sub-intervals in the interior of $[-1/2, +1/2]$, every two adjacent interior sub-intervals covering one period of T_n, plus one interval for each end point. The integral on each sub-interval is computed by using adaptive quadrature [47]. With Macleod's scheme [41], we can accurately compute $\{b_m\}$ in the right-hand-side of Eq. (5) and some parts needed in the elements of matrix A. The details of evaluation of the integral is described in Appendix C.

The third part of the calculation is to invert the dense matrix A in Eq. (5). Since the size of the matrix A is moderate – it is at most 2048×2048 in the present work, it is reasonable to use the direct method. We apply LU decomposition with pivoting to decompose the matrix A and solve for the resulting system by using forward elimination and backward substitution algorithm. To ensure the solution to be accurate up to at least double precision, we implement the algorithms for the LU decomposition, the forward elimination, and the backward substitution by using C++/Fortran 90 with arbitrary precision package [48]. We use 40 digits in the inversion of A and this is the only place where we have to use arbitrary precision package. All other calculations are carried out with double-precision arithmetic.

3. Results and discussion

We numerically solve the integral Eq. (2a) of $u(y,k)$ for the Couette flow with a wide range of the Knudsen number k, *i.e.*, $0.003 \leqslant k \leqslant 10.0$, which spans more than four decades. We vary the size of the linear system, $N^2, N = 2^n$, for $4 \leqslant n \leqslant 11$, *i.e.*, $16 \leqslant N \leqslant 2048$, to ensure the convergence of the results. In what follows we will report numerical results and their analysis. It should also be mentioned that, for numerical efficiency and accuracy, the Clenshaw algorithm [49] must be used to compute sums of Chebyshev polynomials, such as Eq. (3).

3.1. Convergence

We compute the local relative error of the velocity $u(y,k)$ at a specific location y and a given value of k:

$$|\delta u_N(y,k)| := \frac{|u_N(y,k) - u_*(y,k)|}{|u_*(y,k)|}, \tag{7}$$

where the reference solution $u_*(y,k)$ is obtained with $N = 2048$. We compute $|\delta u_N(y,k)|$ at $y = 0.1$, 0.2, 0.4, and 0.5, and $0.003 \leqslant k \leqslant 10.0$. Fig. 2 shows the log–log plots of N-dependence of $|\delta u_N|$ at $y = 0.1$ and $k = 0.01$, $y = 0.2$ and $k = 0.1$, $y = 0.3$ and $k = 1.0$, and $y = 0.4$ and $k = 10.0$. The results indicate that

$$\ln\frac{|\delta u_N(y,k)|}{|\delta u_M(y,k)|} \sim -\alpha \ln\frac{N}{M}, \tag{8}$$

where $N \neq M < 2048$.

Table 1 shows the dependence of α and its standard deviation $\Delta\alpha$ on k. We observe that the rate of convergence α is independent of position y with $0.1 \leqslant y \leqslant 0.5$ and is only dependent on the Knudsen number k. For small values of k, *i.e.*, $k < 1.0$, the rate of convergence α increases as k does, then it exceeds 4.0 and stays constant after $k \geqslant 1.0$. Clearly our scheme is indeed of high-order. The cases of small k converge slightly slower than all the cases of larger $k \geqslant 1.0$. This is expected because the Knudsen layer becomes thinner and thinner as k becomes smaller and smaller, thus it requires more and more collocation points near the end points $y = \pm 1/2$, which is a typical problem encountered in the numerical solutions of the kinetic equation for small Knudsen number k. This is clearly seen in Eq. (1a) – near the boundary, $u(y,k)$ is approximately a function δ/k, where $\delta := |1/2 \pm y|$ is the distance to the end points $y = \pm 1/2$. This issue will be further discussed later in the next section. The rate of convergence clearly indicate that our method is a high-order one.

We next compute the global relative L_2 error of the velocity $u_N(y)$:

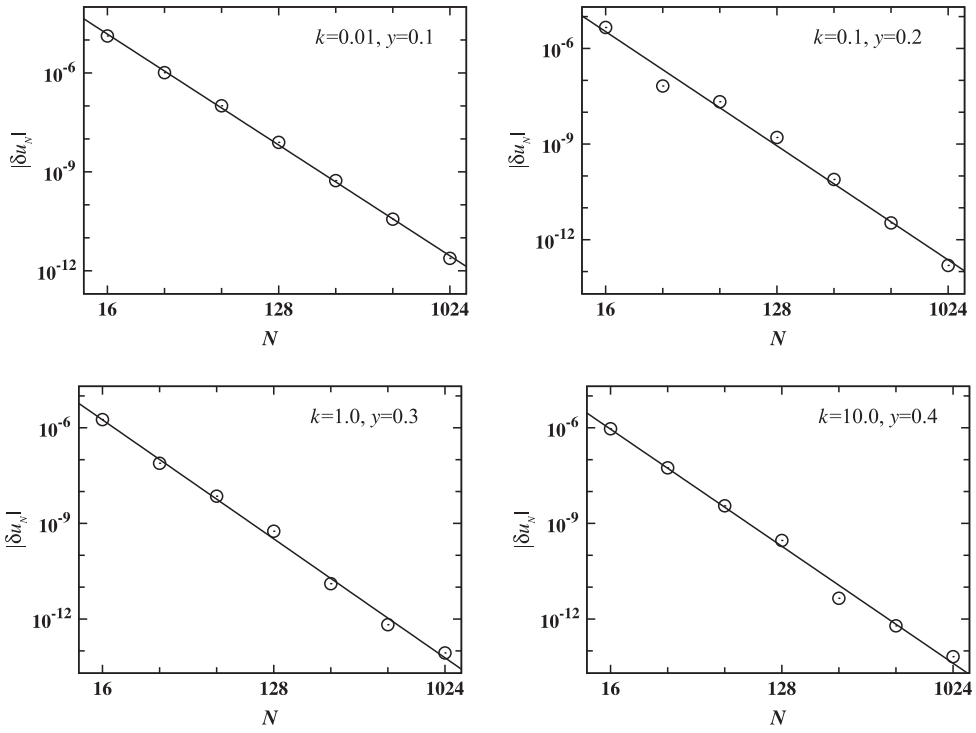

Fig. 2. The grid size N dependence of the relative error of the velocity, $|\delta u_N(y,k)|$. Top row, from left to right: $k = 0.01$ at $y = 0.1$, and $k = 0.1$ at $y = 0.2$. Bottom row, from left to right: $k = 1.0$ at $y = 0.3$, and $k = 10.0$ at $y = 0.4$.

Table 1
The dependence of the rate of convergence, α, for the velocity $u_N(y)$ on the Knudsen number k. The rate of convergence α and its standard deviation are computed by using the least-square fitting.

k	0.003	0.01	0.03	0.1	1.0
$\alpha \pm \Delta\alpha$	3.5559 ± 0.0821	3.7229 ± 0.0586	3.8682 ± 0.0978	3.9660 ± 0.2486	4.1325 ± 0.1567
k	2.0	3.0	5.0	7.0	10.0
$\alpha \pm \Delta\alpha$	4.0949 ± 0.1580	4.0844 ± 0.1668	4.0705 ± 0.1793	4.0709 ± 0.1829	4.0651 ± 0.1881

$$\|\delta u_N(k)\|_2 := \frac{\left[\int_{-1/2}^{1/2} |u_N(y,k) - u_*(y,k)|^2 \mathrm{d}y\right]^{1/2}}{\left[\int_{-1/2}^{1/2} |u_*(y,k)|^2 \mathrm{d}y\right]^{1/2}}, \tag{9}$$

where the reference solution $u_*(y,k)$ is obtained with $N = 2048$. The results of $\|\delta u_N(k)\|_2$ with $k = 0.003$, 0.01, 0.03, 0.1, 1.0, and 10.0 are given in Table 2. The global L_2 error $\|\delta u_N(k)\|_2$ shows very weak dependence on k. For all values of $0.003 \leqslant k \leqslant 10.0$, the rate of convergence $\alpha > 3$, indicating again that the scheme is of high-order.

3.2. The flow velocity $u(y,k)$, the shear stress $P_{xy}(k)$, and the half-channel total mass flow rate $Q(k)$

In this section we present our results for the velocity $u_N(y,k)$ with $0.003 \leqslant k \leqslant 10.0$. For each value of k, we solve Eq. (2a) with $16 \leqslant N \leqslant 2048$. All calculations are carried out with double-precision arithmetic unless otherwise stated.

We compile two tables to summarize the numerical results related to the velocity $u(y,k)$. Table 3 compiles the values of $u_N(y,k)$ at $y = 0.1$, 0.2, 0.3, 0.4, and 0.5. At channel center $y = 0, u_N(0,k) = 0$. For all cases of k, the results of $u(y,k)$ are accurate for at the least eleven (11) significant digits. In addition, Table 4 compiles the values of the velocity at the boundary, $u(1/2,k)$, and the derivative of the velocity at the channel center, $u'(0,k)$. Both $u(1/2,k)$ and $u'(0,k)$ decrease monotonically as k increases. Also, the normalized derivative, $u'(0,k)/u(1/2,k)$, decreases monotonically as k increases. The data of $u(1/2,k)$ and $u'(0,k)$ will be used later to construct approximated solutions for $u(y,k)$ and other quantities.

The accurate solutions of $u_N(y,k)$ allow us to obtain accurate shear stress P_{xy} and the half-channel mass flow rate (for the upper half channel) Q. The shear stress P_{xy} normalized by $2Up_0/c_\mathrm{m} = 2U\rho_0 RT_0/c_\mathrm{m}$ is

$$P_{xy}(y,k) = \frac{1}{\sqrt{\pi}} \int_{-\infty}^{\infty} \phi \xi_y e^{-\xi_y^2} \mathrm{d}\xi_y, \tag{10}$$

where $\phi(y,\xi_y)$ and its relation with the velocity u are given by

$$\xi_y \frac{\partial \phi}{\partial y} = -\frac{1}{k}[\phi - u], \tag{11a}$$

$$u = \frac{1}{\sqrt{\pi}} \int_{-\infty}^{\infty} \phi e^{-\xi_y^2} \mathrm{d}\xi_y. \tag{11b}$$

It is easy to prove that P_{xy} is a constant independent of y, with a fixed value of k, because [2]:

$$\frac{\partial P_{xy}}{\partial y} = \frac{1}{\sqrt{\pi}} \int_{-\infty}^{\infty} \frac{\partial \phi}{\partial y} \xi_y e^{-\xi_y^2} \mathrm{d}\xi_y = -\frac{1}{k\sqrt{\pi}} \int_{-\infty}^{\infty} (\phi - u) e^{-\xi_y^2} \mathrm{d}\xi_y = 0. \tag{12}$$

The value of P_{xy} can be obtained as the following:

$$P_{xy} = \frac{1}{\sqrt{\pi}} \left[\frac{1}{k} \int_{-1/2}^{1/2} I_0\left(\frac{|y-s|}{k}\right) \mathrm{sgn}(y-s) u(s) \mathrm{d}s - \frac{G_1(y,k)}{2}\right]. \tag{13}$$

Table 2
The global relative L_2 error of the velocity $u_N(y)$ and the rate of convergence α.

k	N	$\|\delta u_N(k)\|_2$	k	N	$\|\delta u_N(k)\|_2$
0.003	16	$9.073159564311592 \cdot 10^{-5}$	0.01	16	$6.850638233262458 \cdot 10^{-5}$
	32	$1.173595294063363 \cdot 10^{-5}$		32	$1.158034979497339 \cdot 10^{-5}$
	64	$1.998332365494139 \cdot 10^{-6}$		64	$2.040512264077090 \cdot 10^{-6}$
	128	$3.555748458719578 \cdot 10^{-7}$		128	$3.589887685163785 \cdot 10^{-7}$
	256	$6.318807893148573 \cdot 10^{-8}$		256	$6.336243964057072 \cdot 10^{-8}$
	512	$1.167675652196907 \cdot 10^{-8}$		512	$1.168038817604225 \cdot 10^{-8}$
	1024	$2.398181505564065 \cdot 10^{-9}$		1024	$2.396621872127319 \cdot 10^{-9}$
	α	3.3570		α	3.4584
0.03	16	$6.906363108665610 \cdot 10^{-5}$	0.1	16	$7.023168944878657 \cdot 10^{-5}$
	32	$1.186616010647807 \cdot 10^{-5}$		32	$1.176707411570782 \cdot 10^{-6}$
	64	$2.056433398329269 \cdot 10^{-6}$		64	$2.015858660824019 \cdot 10^{-6}$
	128	$3.588564081981813 \cdot 10^{-7}$		128	$3.503976368566796 \cdot 10^{-7}$
	256	$6.316031862395808 \cdot 10^{-8}$		256	$6.159685518862506 \cdot 10^{-8}$
	512	$1.163297719138161 \cdot 10^{-8}$		512	$1.134097387572629 \cdot 10^{-8}$
	1024	$2.386153226120782 \cdot 10^{-9}$		1024	$2.325951729127107 \cdot 10^{-9}$
	α	3.4554		α	3.4494
1.0	16	$5.455348234878563 \cdot 10^{-5}$	10.0	16	$3.217798103809692 \cdot 10^{-5}$
	32	$8.956151509566837 \cdot 10^{-6}$		32	$5.264751883741950 \cdot 10^{-6}$
	64	$1.524372937533699 \cdot 10^{-6}$		64	$8.952332255181793 \cdot 10^{-7}$
	128	$2.644513283117079 \cdot 10^{-7}$		128	$1.552658662784406 \cdot 10^{-7}$
	256	$4.646189890073849 \cdot 10^{-8}$		256	$2.727692020475305 \cdot 10^{-8}$
	512	$8.553006371558081 \cdot 10^{-9}$		512	$5.021210272459947 \cdot 10^{-9}$
	1024	$1.754065729796481 \cdot 10^{-9}$		1024	$1.029752165284958 \cdot 10^{-9}$
	α	3.5405		α	3.7309

Because P_{xy} is a constant independent of y, we can set $y = 0$ in Eq. (13) so that

$$P_{xy} = -\frac{1}{\sqrt{\pi}}\left[\frac{2}{k}\int_0^{1/2} I_0(s/k)u(s)\mathrm{d}s + I_1(1/2k)\right]. \tag{14}$$

Thus, when $k \to \infty$, the asymptotic value of $P_{xy}(k) = -1/2\sqrt{\pi} \approx -0.282094792$. Also, it can be shown that $P_{xy}(k) \to 0$ as $k \to 0$. Thus $0 \geqslant P_{xy}(k) > -1/2\sqrt{\pi}$.

The half-channel mass flow rate is defined as

$$Q(k) = \int_0^{1/2} u(y,k)\mathrm{d}y. \tag{15}$$

With the Chebyshev expansion of $u(y,k)$ given by Eq. (3), we have:

$$Q_N(k) = \frac{1}{2}\sum_{j=1}^{N}\frac{c_{2j-1}(k)}{1-(-1)^j(2j-1)}. \tag{16}$$

The values of both P_{xy} and Q computed from Eqs. (14) and (16), respectively, are given in Table 5. The results in the table have at least eleven digits of accuracy. Our results given in Tables 3–5 are consistent with the most recent and accurate results for steady Couette flow [25].

3.3. Approximations of velocity $u(y,k)$

In this section we will first explore the features of the velocity $u(y,k)$ and then construct approximations of it. Fig. 3 shows the Knudsen number dependence of the velocity $u(y,k)$. In the figure we compare the velocity $u(y,k)$ of the integral Eq. (2a) obtained by the collocation method with $N = 2048$ and the straight line $u_1(y,k) = u'(0,k)y$, which is tangent to $u(y,k)$ at the channel center $y = 0$. The straight line $u_1(y,k) = u'(0,k)y$ is also a solution of the Navier–Stokes equation with a given slip velocity. The figure shows that in the flow domain about the channel center $y = 0$, the velocity $u(y,k)$ is very close to the hydrodynamic solution $u_1(y,k)$.

To measure the kinetic component of the velocity, we compute the nonlinear component of $u(y,k)/u(1/2,k)$,

$$u_{\mathrm{NL}} := \frac{u(y,k)}{u(1/2,k)} - 2y. \tag{17}$$

As shown in Fig. 3, the nonlinear component of $u(y,k)/u(1/2,k)$ increases as k increases. While it is not obvious in the figure, it can be proved that $u'(y,k)$ does not exist at the boundaries $y = \pm 1/2$, that is, the velocity profile $u(y,k)$ is tangent to the boundaries $y = \pm 1/2$. (The proof of $u'(y,k) \to \pm\infty$ as $y \to \pm 1/2$ is given in Appendix B.) In what follows, we will construct approximations of $u(y,k)$ which will retain some features of $u(y,k)$ based on a set of specified criteria.

In the case of zero Knudsen number, *i.e.*, $k = 0$, the velocity $u(y)$ is a solution of steady Stokes equation which is a linear function of y, and with the normalizations given in Section 2, it is:

$$u_0(y) = y, \quad -1/2 \leqslant y \leqslant +1/2. \tag{18}$$

The kinetic solution $u(y,k)$ deviates from the Stokes solution $u_0(y)$ especially at large Knudsen number k. First, there is a slip velocity u_s at the wall, *i.e.*, the velocity $u(y,k)$ at the wall is *not* equal to the wall velocity U_w. And second, the velocity profile $u(y,k)$ is nonlinear as shown in Fig. 3; there is a Knudsen layer near the walls. The accurate solutions of $u(y,k)$ obtained in the preceding section allows us to gain some insights on the Knudsen layer quantitatively. To do so, we need to define several quantities.

The slope of $u(y,k)$ at the center of the channel is an important quantity to characterize $u(y,k)$ and can be accurately obtained from the Chebyshev expansion of $u_N(y,k)$:

$$u'(0,k) = -2\sum_{j=1}^{N}(-1)^j(2j-1)c_{2j-1}(k). \tag{19}$$

We define the following hydrodynamic solution:

$$u_1(y,k) := u'(0,k)y. \tag{20}$$

While Eq. (20) is linear, however, the slope $u'(0,k)$ is defined by the kinetic solution $u(y,k)$ at $y = 0$. The hydrodynamic solution defined by Eq. (20) is the straight line tangent to $u(y,k)$ at the channel

Table 3
The values of the velocity $u_N(y,k)$ at $y = 0.1$, 0.2, 0.3, 0.4, and 0.5, for $0.003 \leqslant k \leqslant 10.0$ and $256 \leqslant N \leqslant 2048$.

y	0.1	0.2	0.3	0.4	0.5
N	$k = 0.003$				
256	$9.93939802817675 \cdot 10^{-2}$	$1.98787960563724 \cdot 10^{-1}$	$2.98181940854607 \cdot 10^{-1}$	$3.97575921205698 \cdot 10^{-1}$	$4.97891532817256 \cdot 10^{-1}$
512	$9.93939801575752 \cdot 10^{-2}$	$1.98787960322574 \cdot 10^{-1}$	$2.98181940467945 \cdot 10^{-1}$	$3.97575920708319 \cdot 10^{-1}$	$4.97891535105931 \cdot 10^{-1}$
1024	$9.93939801487210 \cdot 10^{-2}$	$1.98787960304567 \cdot 10^{-1}$	$2.98181940443658 \cdot 10^{-1}$	$3.97575920673503 \cdot 10^{-1}$	$4.97891535267197 \cdot 10^{-1}$
2048	$9.93939801484713 \cdot 10^{-2}$	$1.98787960303896 \cdot 10^{-1}$	$2.98181940442773 \cdot 10^{-1}$	$3.97575920671607 \cdot 10^{-1}$	$4.97891535278427 \cdot 10^{-1}$
	$k = 0.01$				
256	$9.80081002587778 \cdot 10^{-2}$	$1.96016201408749 \cdot 10^{-1}$	$2.94024342763042 \cdot 10^{-1}$	$3.92035572153263 \cdot 10^{-1}$	$4.93069779961988 \cdot 10^{-1}$
512	$9.80081002254805 \cdot 10^{-2}$	$1.96016201348442 \cdot 10^{-1}$	$2.94024342646767 \cdot 10^{-1}$	$3.92035572014922 \cdot 10^{-1}$	$4.93069780717902 \cdot 10^{-1}$
1024	$9.80081002231047 \cdot 10^{-2}$	$1.96016201342903 \cdot 10^{-1}$	$2.94024342640619 \cdot 10^{-1}$	$3.92035572003626 \cdot 10^{-1}$	$4.93069780770369 \cdot 10^{-1}$
2048	$9.80081002229763 \cdot 10^{-2}$	$1.96016201342550 \cdot 10^{-1}$	$2.94024342640308 \cdot 10^{-1}$	$3.92035572002762 \cdot 10^{-1}$	$4.93069780773982 \cdot 10^{-1}$
	$k = 0.03$				
256	$9.42551023448203 \cdot 10^{-2}$	$1.88515596522206 \cdot 10^{-1}$	$2.82808471818603 \cdot 10^{-1}$	$3.77352560943944 \cdot 10^{-1}$	$4.80005867993200 \cdot 10^{-1}$
512	$9.42551023372640 \cdot 10^{-2}$	$1.88515596512985 \cdot 10^{-1}$	$2.82808471779802 \cdot 10^{-1}$	$3.77352560907856 \cdot 10^{-1}$	$4.80005868257133 \cdot 10^{-1}$
1024	$9.42551023364727 \cdot 10^{-2}$	$1.88515596510692 \cdot 10^{-1}$	$2.82808471778404 \cdot 10^{-1}$	$3.77352560903030 \cdot 10^{-1}$	$4.80005868275276 \cdot 10^{-1}$
2048	$9.42551023363842 \cdot 10^{-2}$	$1.88515596510505 \cdot 10^{-1}$	$2.82808471778333 \cdot 10^{-1}$	$3.77352560902472 \cdot 10^{-1}$	$4.80005868276515 \cdot 10^{-1}$
	$k = 0.1$				
256	$8.35610402937810 \cdot 10^{-2}$	$1.67349050225909 \cdot 10^{-1}$	$2.51810807114286 \cdot 10^{-1}$	$3.38368406078662 \cdot 10^{-1}$	$4.41224640891364 \cdot 10^{-1}$
512	$8.35610402944326 \cdot 10^{-2}$	$1.67349050232477 \cdot 10^{-1}$	$2.51810807101969 \cdot 10^{-1}$	$3.38368406075732 \cdot 10^{-1}$	$4.41224640966721 \cdot 10^{-1}$
1024	$8.35610402942453 \cdot 10^{-2}$	$1.67349050231428 \cdot 10^{-1}$	$2.51810807102181 \cdot 10^{-1}$	$3.38368406073280 \cdot 10^{-1}$	$4.41224640971868 \cdot 10^{-1}$
2048	$8.35610402942564 \cdot 10^{-2}$	$1.67349050231355 \cdot 10^{-1}$	$2.51810807102247 \cdot 10^{-1}$	$3.38368406072997 \cdot 10^{-1}$	$4.41224640972217 \cdot 10^{-1}$
	$k = 0.3$				
256	$6.64543006930748 \cdot 10^{-2}$	$1.33570950940784 \cdot 10^{-1}$	$2.02360723344343 \cdot 10^{-1}$	$2.75170669357004 \cdot 10^{-1}$	$3.67212569528701 \cdot 10^{-1}$
512	$6.64543006949853 \cdot 10^{-2}$	$1.33570950948607 \cdot 10^{-1}$	$2.02360723339400 \cdot 10^{-1}$	$2.75170669360757 \cdot 10^{-1}$	$3.67212569548601 \cdot 10^{-1}$
1024	$6.64543006949260 \cdot 10^{-2}$	$1.33570950947971 \cdot 10^{-1}$	$2.02360723339812 \cdot 10^{-1}$	$2.75170669359285 \cdot 10^{-1}$	$3.67212569549952 \cdot 10^{-1}$
2048	$6.64543006949395 \cdot 10^{-2}$	$1.33570950947927 \cdot 10^{-1}$	$2.02360723339879 \cdot 10^{-1}$	$2.75170669359094 \cdot 10^{-1}$	$3.67212569550043 \cdot 10^{-1}$
	$k = 1.0$				
256	$4.45319411508086 \cdot 10^{-2}$	$8.97629000550284 \cdot 10^{-2}$	$1.36669180693308 \cdot 10^{-1}$	$1.87233642995143 \cdot 10^{-1}$	$2.51861339985755 \cdot 10^{-1}$
512	$4.45319411521308 \cdot 10^{-2}$	$8.97629000599260 \cdot 10^{-2}$	$1.36669180691337 \cdot 10^{-1}$	$1.87233642998431 \cdot 10^{-1}$	$2.51861339989221 \cdot 10^{-1}$
1024	$4.45319411521130 \cdot 10^{-2}$	$8.97629000596012 \cdot 10^{-2}$	$1.36669180691618 \cdot 10^{-1}$	$1.87233642997678 \cdot 10^{-1}$	$2.51861339989455 \cdot 10^{-1}$
2048	$4.45319411521217 \cdot 10^{-2}$	$8.97629000595787 \cdot 10^{-2}$	$1.36669180691658 \cdot 10^{-1}$	$1.87233642997577 \cdot 10^{-1}$	$2.51861339989471 \cdot 10^{-1}$
	$k = 2.0$				
256	$3.28317510127771 \cdot 10^{-2}$	$6.62008086650869 \cdot 10^{-2}$	$1.00839934023394 \cdot 10^{-1}$	$1.38179710139242 \cdot 10^{-1}$	$1.85246299372828 \cdot 10^{-1}$
512	$3.28317510136486 \cdot 10^{-2}$	$6.62008086682613 \cdot 10^{-2}$	$1.00839934022253 \cdot 10^{-1}$	$1.38179710141497 \cdot 10^{-1}$	$1.85246299373941 \cdot 10^{-1}$
1024	$3.28317510136395 \cdot 10^{-2}$	$6.62008086680595 \cdot 10^{-2}$	$1.00839934022438 \cdot 10^{-1}$	$1.38179710141030 \cdot 10^{-1}$	$1.85246299374016 \cdot 10^{-1}$
2048	$3.28317510136450 \cdot 10^{-2}$	$6.62008086680455 \cdot 10^{-2}$	$1.00839934022465 \cdot 10^{-1}$	$1.38179710140967 \cdot 10^{-1}$	$1.85246299374021 \cdot 10^{-1}$
	$k = 3.0$				
256	$2.67884225065252 \cdot 10^{-2}$	$5.40076130212065 \cdot 10^{-2}$	$8.22393190026562 \cdot 10^{-2}$	$1.12600645437724 \cdot 10^{-1}$	$1.50428244498615 \cdot 10^{-1}$
512	$2.67884225071785 \cdot 10^{-2}$	$5.40076130235737 \cdot 10^{-2}$	$8.22393190018391 \cdot 10^{-2}$	$1.12600645439436 \cdot 10^{-1}$	$1.50428244499167 \cdot 10^{-1}$
1024	$2.67884225071721 \cdot 10^{-2}$	$5.40076130234255 \cdot 10^{-2}$	$8.22393190019777 \cdot 10^{-2}$	$1.12600645439093 \cdot 10^{-1}$	$1.50428244499204 \cdot 10^{-1}$
2048	$2.67884225071763 \cdot 10^{-2}$	$5.40076130234154 \cdot 10^{-2}$	$8.22393190019973 \cdot 10^{-2}$	$1.12600645439046 \cdot 10^{-1}$	$1.50428244499207 \cdot 10^{-1}$
	$k = 5.0$				
256	$2.02181035056891 \cdot 10^{-2}$	$4.07451054936705 \cdot 10^{-2}$	$6.19942703911553 \cdot 10^{-2}$	$8.47465578276147 \cdot 10^{-2}$	$1.12635188029221 \cdot 10^{-1}$
512	$2.02181035061279 \cdot 10^{-2}$	$4.07451054952536 \cdot 10^{-2}$	$6.19942703906268 \cdot 10^{-2}$	$8.47465578287766 \cdot 10^{-2}$	$1.12635188029443 \cdot 10^{-1}$
1024	$2.02181035061240 \cdot 10^{-2}$	$4.07451054951556 \cdot 10^{-2}$	$6.19942703907201 \cdot 10^{-2}$	$8.47465578285502 \cdot 10^{-2}$	$1.12635188029458 \cdot 10^{-1}$
2048	$2.02181035061269 \cdot 10^{-2}$	$4.07451054951488 \cdot 10^{-2}$	$6.19942703907331 \cdot 10^{-2}$	$8.47465578285188 \cdot 10^{-2}$	$1.12635188029459 \cdot 10^{-1}$
	$k = 7.0$				
256	$1.65589614002174 \cdot 10^{-2}$	$3.33595222277592 \cdot 10^{-2}$	$5.07233582368858 \cdot 10^{-2}$	$6.92533624010780 \cdot 10^{-2}$	$9.17168961350864 \cdot 10^{-2}$
512	$1.65589614005492 \cdot 10^{-2}$	$3.33595222289539 \cdot 10^{-2}$	$5.07233582364927 \cdot 10^{-2}$	$6.92533624019604 \cdot 10^{-2}$	$9.17168961352056 \cdot 10^{-2}$
1024	$1.65589614005463 \cdot 10^{-2}$	$3.33595222288803 \cdot 10^{-2}$	$5.07233582365632 \cdot 10^{-2}$	$6.92533624017904 \cdot 10^{-2}$	$9.17168961352137 \cdot 10^{-2}$
2048	$1.65589614005484 \cdot 10^{-2}$	$3.33595222288753 \cdot 10^{-2}$	$5.07233582365731 \cdot 10^{-2}$	$6.92533624017670 \cdot 10^{-2}$	$9.17168961352143 \cdot 10^{-2}$
	$k = 10.0$				
256	$1.32484005418904 \cdot 10^{-2}$	$2.66795457529754 \cdot 10^{-2}$	$4.05357403215398 \cdot 10^{-2}$	$5.52678934659797 \cdot 10^{-2}$	$7.29221129932192 \cdot 10^{-2}$
512	$1.32484005421342 \cdot 10^{-2}$	$2.66795457538518 \cdot 10^{-2}$	$4.05357403212547 \cdot 10^{-2}$	$5.52678934666303 \cdot 10^{-2}$	$7.29221129932804 \cdot 10^{-2}$
1024	$1.32484005421322 \cdot 10^{-2}$	$2.66795457537980 \cdot 10^{-2}$	$4.05357403213064 \cdot 10^{-2}$	$5.52678934665059 \cdot 10^{-2}$	$7.29221129932845 \cdot 10^{-2}$
2048	$1.32484005421337 \cdot 10^{-2}$	$2.66795457537942 \cdot 10^{-2}$	$4.05357403213135 \cdot 10^{-2}$	$5.52678934664887 \cdot 10^{-2}$	$7.29221129932848 \cdot 10^{-2}$

Table 4
The dependence of the velocity at boundary $y = 1/2, u(1/2,k)$, and the velocity derivative at the channel center $y = 0$, $u'(0,k)$, on the Knudsen number k. The results are obtained with the Chebyshev expansion with $N = 2048$.

k	$u(1/2,k)$	$u'(0,k)$
0.003	$4.97891535278427 \cdot 10^{-1}$	0.993939801103754
0.01	$4.93069780773982 \cdot 10^{-1}$	0.980081001908009
0.03	$4.80005868276515 \cdot 10^{-1}$	0.942545599824700
0.1	$4.41224640972217 \cdot 10^{-1}$	0.835285765647133
0.3	$3.67212569550043 \cdot 10^{-1}$	0.663530077027944
1.0	$2.51861339989471 \cdot 10^{-1}$	0.444228469746625
2.0	$1.85246299374021 \cdot 10^{-1}$	0.327474576937359
3.0	$1.50428244499207 \cdot 10^{-1}$	0.267207005940212
5.0	$1.12635188029459 \cdot 10^{-1}$	0.201694431817770
7.0	$9.17168961352143 \cdot 10^{-2}$	0.165208634795606
10.0	$7.29221129932848 \cdot 10^{-2}$	0.132195579051697

Table 5
The dependence of the stress P_{xy} and the total mass flow rate Q on the Knudsen number k.

k	$P_{xy}(k)$	$Q(k)$
0.003	$-1.490909702173263 \cdot 10^{-3}$	$1.242445655358978 \cdot 10^{-1}$
0.01	$-4.900405009668500 \cdot 10^{-3}$	$1.225330275294396 \cdot 10^{-1}$
0.03	$-1.413798601517447 \cdot 10^{-2}$	$1.180147037185861 \cdot 10^{-1}$
0.1	$-4.155607782559217 \cdot 10^{-2}$	$1.057028408172310 \cdot 10^{-1}$
0.3	$-9.344983511356993 \cdot 10^{-2}$	$8.560111699820641 \cdot 10^{-2}$
1.0	$-1.694625753368235 \cdot 10^{-1}$	$5.804708735555424 \cdot 10^{-2}$
2.0	$-2.083322536749378 \cdot 10^{-1}$	$4.281659776113900 \cdot 10^{-2}$
3.0	$-2.266437497658086 \cdot 10^{-1}$	$3.489298506190797 \cdot 10^{-2}$
5.0	$-2.446632678455995 \cdot 10^{-1}$	$2.627042060967372 \cdot 10^{-2}$
7.0	$-2.536943539674480 \cdot 10^{-1}$	$2.147460412330824 \cdot 10^{-2}$
10.0	$-2.611624603488405 \cdot 10^{-1}$	$1.714449048590636 \cdot 10^{-2}$

center $y = 0$. The linear profile defined by Eq. (20) can be seen as the hydrodynamic component of the velocity $u(y,k)$.

By substituting the following linear approximation of $u(y,k)$

$$\tilde{u}_0(y,k) = \frac{y}{1 + k\sqrt{\pi/2}}, \tag{21}$$

into the right-hand-side of the integral Eq. (1a), we can obtain an approximated solution of $u(y,k)$ to illustrate its nonlinearity and the singular nature of the Knudsen layer near the boundary [9]:

$$\tilde{u}(y,k) = \frac{k}{1 + k\sqrt{\pi/2}}\left\{\frac{y}{k} + \frac{F_0(y,k)}{2\sqrt{2}} - \frac{F_1(y,k)}{\sqrt{\pi}}\right\}, \tag{22}$$

where $F_n(y,k)$ is defined in Eq. (1c). Near the wall at $y = +1/2$, $\delta := (1/2 - y) \ll 1$, then both $I_n((1/2+y)/k) = I_n((1-\delta)/k) \approx I_n(1/k)$ and $I_n((1/2-y)/k) = I_n(\delta/k)$ can be approximated by their leading order expansions [41], which are given in Appendix A, thus Eq. (22) becomes:

$$\begin{aligned}\tilde{u}(y,k) &\approx \frac{k}{1 + k\sqrt{\pi/2}}\left\{\frac{1}{2}(\delta/k) + \frac{1}{2\sqrt{2}}(\delta/k)\ln(\delta/k)\right.\\ &\quad\left. + \frac{1}{2k} + \left(\frac{\sqrt{\pi}}{4\sqrt{2}} - \frac{1}{2\sqrt{\pi}} - \frac{1}{2\sqrt{2}}I_0(1/k) + \frac{1}{\sqrt{\pi}}I_1(1/k)\right)\right\}\\ &= a_0(\delta/k)\left[1 + \frac{1}{\sqrt{2}}\ln(\delta/k)\right] + \tilde{u}(1/2,k),\end{aligned} \tag{23a}$$

$$\begin{aligned}\tilde{u}(1/2,k) &:= a_0\left\{\frac{1}{k} + \frac{2}{\sqrt{\pi}}F_1(0,k) - \frac{1}{\sqrt{2}}F_0(0,k)\right\}\\ &= a_0\left\{\frac{1}{k} + \left[\frac{\sqrt{\pi}}{2\sqrt{2}} - \frac{1}{\sqrt{\pi}} - \frac{1}{\sqrt{2}}I_0(1/k) + \frac{2}{\sqrt{\pi}}I_1(1/k)\right]\right\},\end{aligned} \tag{23b}$$

$$a_0 := \frac{k}{2 + k\sqrt{2\pi}}. \tag{23c}$$

Eq. (23a) manifests the leading order singularity of $u(y,k)$ at the boundary $y = \pm 1/2$ is $(\delta/k)\ln(\delta/k)$ with $\delta := 1/2 \mp y$. Clearly, when $y \to \pm 1/2, u'(y,k) \sim \ln(\delta/k)$, thus $u'(y,k)$ does not exist at the boundaries $y = \pm 1/2$ for $k \neq 0$. While the approximated solution $\tilde{u}(y,k)$ reveals the singular nature of $u(y,k)$, it does not approximate $u(y,k)$ well quantitatively. For instance, $\tilde{u}(1/2,k) \neq u(1/2,k)$ and $\tilde{u}'(0,k) \neq u'(0,k)$.

We can improve the approximation of $u(y,k)$ based on $\tilde{u}(y,k)$ by assuming that the approximation of $u(y,k)$ has the following form:

$$\tilde{u}_1(y,k) = A(k)y + B(k)F_0(y,k) + C(k)F_1(y,k), \tag{24}$$

where $A(k), B(k)$, and $C(k)$ are functions of k alone and are fully determined by the following constraints on $\tilde{u}_1(y,k)$:

$$\tilde{u}_1(1/2,k) = u(1/2,k), \tag{25a}$$

$$\tilde{u}_1'(0,k) = u'(0,k), \tag{25b}$$

$$\int_0^{1/2} \tilde{u}_1(y,k)\mathrm{d}y = Q(k), \tag{25c}$$

where $u(1/2,k), u'(0,k)$, and $Q(k)$ are obtained by using the accurate solutions $u_N(y,k)$ of the integral Eq. (2a) presented in the previous section. Specifically, the equations for A, B, and C are:

$$A + \frac{2}{k}I_{-1}(1/2k)B + \frac{2}{k}I_0(1/2k)C = u'(0,k), \tag{26a}$$

$$\frac{1}{2}A + \left[\frac{\sqrt{\pi}}{2} - I_0(1/k)\right]B + \left[\frac{1}{2} - I_1(1/k)\right]C = u(1/2,k), \tag{26b}$$

$$\frac{1}{8}A + k\left[\frac{1}{2} + I_1(1/k) - 2I_1(1/2k)\right]B + k\left[\frac{\sqrt{\pi}}{4} + I_2(1/k) - 2I_2(1/2k)\right]C = Q(k). \tag{26c}$$

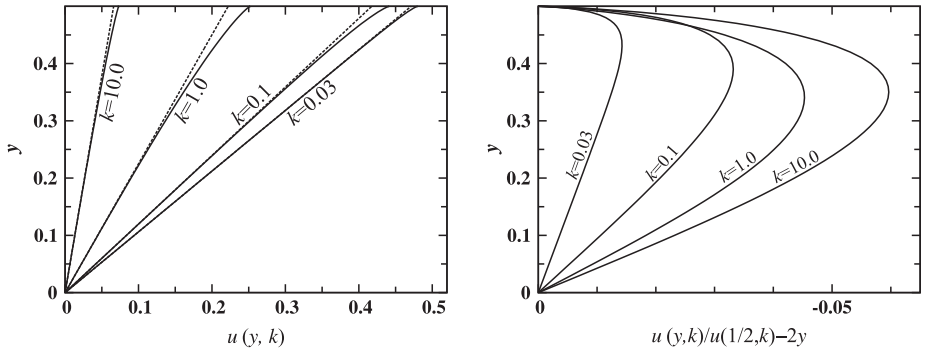

Fig. 3. The Knudsen number k dependence of velocity $u(y,k)$. Left: The solid and dashed lines correspond to the numerical solution $u_N(y,k)$ with $N = 2048$ and $u_1(y,k) = u'(0,k)y$, *i.e.*, the straight line tangent to $u(y,k)$ at $y = 0$. Right: The normalized nonlinear component of the velocity, u_{NL} defined by Eq. (17). $u(y,k)/u(1/2,k)$.

The numerical solutions of $A(k), B(k)$ and $C(k)$ are given in Table 6. The solutions of $A(k), B(k)$ and $C(k)$ show that they are smooth functions of k.

To measure the accuracy and quality of the approximated solution $\tilde{u}_1(y,k)$, we compute the global L_2 error of $\tilde{u}_1(y,k)$ and the shear stress P_{xy} obtained from $\tilde{u}_1(y,k)$, and tabulate the results in Table 7. The half channel mass flow rate Q is used as one of the constraints to determine $\tilde{u}_1(y,k)$, and Q computed from the approximated solution $\tilde{u}_1(y,k)$ is indeed identical to Q computed with $u_N(y,k)$ given in Table 5. The L_2 global error of $\tilde{u}_1(y,k)$ never exceeds $7\cdot 10^{-4}$, and the errors in the stress P_{xy} obtained from $\tilde{u}_1(y,k)$ are in the fifth digit or smaller. Clearly, the approximated solution $\tilde{u}_1(y,k)$ of Eq. (24) is accurate in terms of the above measurements.

The approximated solution $\tilde{u}_1(y,k)$ of Eq. (24) captures the leading-order singularities of $u(y,k)$ at the boundaries. However, to construct boundary conditions of Maxwell's slip-velocity model [42], which can be used in the Navier–Stokes equations [50–53,24,54,55], we cannot allow the boundary singularities in the velocity $u(y,k)$, because these models require derivatives of $u(y,k)$ at the boundary. We can approximate $u(y,k)$ with the following simple cubic polynomial which has the correct symmetry of the flow but without the boundary singularities:

$$\tilde{u}_2(y,k) = u'(0,k)y + a(k)y^3, \quad |y| \leqslant h_0 \leqslant 1/2, \tag{27}$$

where $u'(0,k)$ is given by Eq. (19) and $a(k)$ is the only parameter in $\tilde{u}_2(y,k)$ which is obtained by the least-square fitting of $\tilde{u}_2(y,k)$ to $u(y,k)$. Eq. (27) is inspired by the fact that $u(y,k)$ can be accurately approximated by cubic polynomial through variational approach [12]. We compute $a(k)$ by using different flow domain sizes $|y| \leqslant h_0, h_0 = 0.1, 0.25, 0.4$, and 0.5. The results are given in Table 8.

The coefficient $a(k)$ in Eq. (27) measures the strength of the nonlinear component of the velocity $u(y,k)$. It is interesting to note that the maximum of $a(k)$ occurs at $k = 1.0$ for the values of k with which $u(y,k)$ has been computed. However, if we use the normalized velocity $u(y,k)/u(1/2,k)$, then $a(k)/u(1/2,k)$ increases monotonically with k, as shown in Fig. 3. For almost all cases of $k, a(k)$ increases monotonically as increases the domain size in which $\tilde{u}_2(y,k)$ is used to approximate $u(y,k)$. For all values of $k \in [0.003, 10.0]$, the velocity $u(y,k)$ is very well approximated by the linear profile $u'(0,k)y$ in the flow domain about the channel center – the L_2 global error of $\tilde{u}_2(y,k)$ in the domain of $|y| \leqslant 0.1$ never exceeds $5\cdot 10^{-6}$.

There are other quantities which can be used to measure $\tilde{u}_2(y,k)$ about its accuracy to approximate $u(y,k)$, including the boundary value $\tilde{u}_2(1/2,k)$, the half-channel mass flow rate Q, and the stress P_{xy}. The values of $\tilde{u}_2(1/2,k), Q$, and P_{xy} computed with $\tilde{u}_2(y,k)$ are given in Table 9. Comparing $\tilde{u}_2(1/2,k)$ in Table 9 with the data of $u(1/2,k)$ of Table 4, we see that the errors of

Table 7
The global L_2 error of the approximated $\tilde{u}_1(y,k) = Ay + BF_0(y,k) + CF_1(y,k)$ and the shear stress P_{xy} obtained from $\tilde{u}_1(y,k)$.

k	$\|\delta\tilde{u}_1(k)\|_2$	$P_{xy}(k)$
0.003	$4.1196\cdot 10^{-6}$	$-1.490909701655703\cdot 10^{-3} \pm 5.4872\cdot 10^{-15}$
0.01	$2.8713\cdot 10^{-5}$	$-4.900405009089867\cdot 10^{-3} \pm 2.0275\cdot 10^{-14}$
0.03	$2.8279\cdot 10^{-4}$	$-1.413793251056168\cdot 10^{-2} \pm 5.6901\cdot 10^{-9}$
0.1	$6.8547\cdot 10^{-4}$	$-4.155030609974823\cdot 10^{-2} \pm 2.0460\cdot 10^{-6}$
0.3	$4.8290\cdot 10^{-4}$	$-9.344448147076767\cdot 10^{-2} \pm 5.6934\cdot 10^{-6}$
1.0	$2.0757\cdot 10^{-4}$	$-1.694619104626556\cdot 10^{-1} \pm 2.3569\cdot 10^{-6}$
2.0	$1.1023\cdot 10^{-4}$	$-2.083321401486735\cdot 10^{-1} \pm 8.0488\cdot 10^{-7}$
3.0	$7.3370\cdot 10^{-5}$	$-2.266437144577648\cdot 10^{-1} \pm 3.7549\cdot 10^{-7}$
5.0	$4.2699\cdot 10^{-5}$	$-2.446632605710038\cdot 10^{-1} \pm 1.2894\cdot 10^{-7}$
7.0	$2.9503\cdot 10^{-5}$	$-2.536943515313993\cdot 10^{-1} \pm 6.0449\cdot 10^{-8}$
10.0	$1.9772\cdot 10^{-5}$	$-2.611624596132240\cdot 10^{-1} \pm 2.6077\cdot 10^{-8}$

$\tilde{u}_2(1/2,k)$ are less than 3%. And comparing the data of Q and P_{xy} of Table 9 computed by using $\tilde{u}_2(y,k)$ with the data of Table 5, we can see that the errors of Q are less than 1% and the errors of P_{xy} are less than 0.5%. Thus for practical purposes and in terms of the above measurements, $\tilde{u}_2(y,k)$ is an adequate approximation for $u(y,k)$.

If the derivative $u'(0,k)$ is the quantity of primary concern, then we can use the following approximation for the velocity $u(y,k)$:

$$\tilde{u}_3(y,k) = u'(0,k)y + 4[2u(1/2,k) - u'(0,k)]y^3, \quad |y| \leqslant h_0 \leqslant 1/2. \tag{28}$$

Now there is no fitting parameter in the above approximation of $u(y,k)$; $\tilde{u}_3(1/2,k) = u(1/2,k)$ and $\tilde{u}_3'(0,k) = u'(0,k)$, and both $u(1/2,k)$ and $u'(0,k)$ are provided by the accurate solution of the integral solution (2a) given in Table 4. We compute the L_2 global error, the half-channel total mass flow rate Q, and the stress P_{xy} by using the approximated solution $\tilde{u}_3(y,k)$, and the results are given in Table 10. The L_2 global errors of $\tilde{u}_3(y,k)$ are larger than that of $\tilde{u}_2(y,k)$ given by Eq. (27) by a factor no more than 3; the errors in Q and P_{xy} are also larger than that with $\tilde{u}_2(y,k)$, although they remain relatively small: the errors in Q and P_{xy} are bounded by 2.4% and 0.7%, respectively.

To investigate the possibility of improving the approximation given by Eq. (28), we introduce the following approximation:

$$\tilde{u}_4(y,k) = u'(0,k)y + \left[u(1/2,k) - \frac{1}{2}u'(0,k)\right](2y)^{\gamma}, \quad |y| \leqslant h_0 \leqslant 1/2, \tag{29}$$

where the exponent γ is the only adjustable parameter, which is obtained by the least-square fitting. The results of γ, as well as the results of the L_2 global errors, the half-channel mass flow rate,

Table 6
The numerical solutions of Eq. (26) for the coefficients $A(k), B(k)$ and $C(k)$.

k	A	B	C
0.003	$9.939398011037547\cdot 10^{-1}$	$4.203888321649420\cdot 10^{-4}$	$1.098149648651225\cdot 10^{-3}$
0.01	$9.800810019019697\cdot 10^{-1}$	$1.381929614714690\cdot 10^{-3}$	$3.609153178711989\cdot 10^{-3}$
0.03	$9.425419498579877\cdot 10^{-1}$	$4.117989399334418\cdot 10^{-3}$	$1.017084072395429\cdot 10^{-2}$
0.1	$8.329356170017682\cdot 10^{-1}$	$1.958836369520414\cdot 10^{-2}$	$1.480875860779301\cdot 10^{-2}$
0.3	$6.379645268711726\cdot 10^{-1}$	$6.031742674360471\cdot 10^{-2}$	$-9.010953908070029\cdot 10^{-3}$
1.0	$3.827430174542746\cdot 10^{-1}$	$1.289092270309213\cdot 10^{-1}$	$-9.736027778683470\cdot 10^{-2}$
2.0	$2.644689510083537\cdot 10^{-1}$	$1.695879157944917\cdot 10^{-1}$	$-1.888905977706435\cdot 10^{-1}$
3.0	$2.100280076555217\cdot 10^{-1}$	$1.909461676316779\cdot 10^{-1}$	$-2.568629932617473\cdot 10^{-1}$
5.0	$1.554441376291299\cdot 10^{-1}$	$2.141141551745609\cdot 10^{-1}$	$-3.566589264444766\cdot 10^{-1}$
7.0	$1.267321809253623\cdot 10^{-1}$	$2.269031187313728\cdot 10^{-1}$	$-4.302171682790011\cdot 10^{-1}$
10.0	$1.015072463335740\cdot 10^{-1}$	$2.383573140063627\cdot 10^{-1}$	$-5.141844415188976\cdot 10^{-1}$

Table 8
The coefficient $a(k)$ of the cubic term in $\tilde{u}_2(y,k) = a(k)y^3 + u'(0)y$ and L_2 global error of $\tilde{u}_2(y,k)$.

k	a	$\|\delta u\|_2$
	$0 \leqslant y \leqslant 0.1$	
0.003	$5.099593062063754 \cdot 10^{-8}$	$1.3874 \cdot 10^{-10}$
0.01	$3.343744310958851 \cdot 10^{-8}$	$3.0183 \cdot 10^{-11}$
0.03	$5.281661481222335 \cdot 10^{-4}$	$8.6155 \cdot 10^{-8}$
0.1	$3.221450332360452 \cdot 10^{-2}$	$1.7249 \cdot 10^{-6}$
1.0	$1.087385972974718 \cdot 10^{-1}$	$4.6313 \cdot 10^{-6}$
2.0	$8.404038575996586 \cdot 10^{-2}$	$4.4692 \cdot 10^{-6}$
3.0	$6.752579776310266 \cdot 10^{-2}$	$4.2472 \cdot 10^{-6}$
5.0	$4.852427628554858 \cdot 10^{-2}$	$3.9039 \cdot 10^{-6}$
7.0	$3.799335117677678 \cdot 10^{-2}$	$3.6636 \cdot 10^{-6}$
10.0	$2.876474290181471 \cdot 10^{-2}$	$3.4109 \cdot 10^{-6}$
	$0 \leqslant y \leqslant 0.25$	
0.003	$8.910398731314538 \cdot 10^{-9}$	$1.6440 \cdot 10^{-10}$
0.01	$2.281723886791297 \cdot 10^{-7}$	$4.4609 \cdot 10^{-9}$
0.03	$9.362491604139115 \cdot 10^{-4}$	$6.0262 \cdot 10^{-6}$
0.1	$3.801461087150716 \cdot 10^{-2}$	$8.5867 \cdot 10^{-5}$
1.0	$1.166555192399757 \cdot 10^{-1}$	$2.1281 \cdot 10^{-4}$
2.0	$8.965402727287951 \cdot 10^{-2}$	$2.0421 \cdot 10^{-4}$
3.0	$7.187268534084894 \cdot 10^{-2}$	$1.9367 \cdot 10^{-4}$
5.0	$5.153603790568363 \cdot 10^{-2}$	$1.7772 \cdot 10^{-4}$
7.0	$4.030682982958223 \cdot 10^{-2}$	$1.6667 \cdot 10^{-4}$
10.0	$3.048715410738038 \cdot 10^{-2}$	$1.5511 \cdot 10^{-4}$
	$0 \leqslant y \leqslant 0.4$	
0.003	$3.461904416529674 \cdot 10^{-9}$	$1.5676 \cdot 10^{-10}$
0.01	$1.856312338363668 \cdot 10^{-5}$	$1.7824 \cdot 10^{-6}$
0.03	$3.299567364766678 \cdot 10^{-3}$	$1.4500 \cdot 10^{-4}$
0.1	$5.579151702265811 \cdot 10^{-2}$	$1.0135 \cdot 10^{-3}$
1.0	$1.375949468072168 \cdot 10^{-1}$	$2.0840 \cdot 10^{-3}$
2.0	$1.043359531536905 \cdot 10^{-1}$	$1.9723 \cdot 10^{-3}$
3.0	$8.318922556028895 \cdot 10^{-2}$	$1.8612 \cdot 10^{-3}$
5.0	$5.934281798850302 \cdot 10^{-2}$	$1.7010 \cdot 10^{-3}$
7.0	$4.629066041789258 \cdot 10^{-2}$	$1.5926 \cdot 10^{-3}$
10.0	$3.493410766837902 \cdot 10^{-2}$	$1.4803 \cdot 10^{-3}$
	$0 \leqslant y \leqslant 0.45$	
0.003	$1.019246570609792 \cdot 10^{-7}$	$2.4671 \cdot 10^{-8}$
0.01	$1.451549152540907 \cdot 10^{-4}$	$2.1444 \cdot 10^{-5}$
0.03	$6.572911061238614 \cdot 10^{-3}$	$4.9401 \cdot 10^{-4}$
0.1	$6.996991026752306 \cdot 10^{-2}$	$2.3617 \cdot 10^{-3}$
1.0	$1.517910790377233 \cdot 10^{-1}$	$4.3275 \cdot 10^{-3}$
2.0	$1.141552197717352 \cdot 10^{-1}$	$4.0589 \cdot 10^{-3}$
3.0	$9.071566848876420 \cdot 10^{-2}$	$3.8176 \cdot 10^{-3}$
5.0	$6.450797155323322 \cdot 10^{-2}$	$3.4795 \cdot 10^{-3}$
7.0	$5.023949416869138 \cdot 10^{-2}$	$3.2539 \cdot 10^{-3}$
10.0	$3.786238847877981 \cdot 10^{-2}$	$3.0220 \cdot 10^{-3}$
	$0 \leqslant y \leqslant 0.5$	
0.003	$1.004492580134579 \cdot 10^{-3}$	$4.1487 \cdot 10^{-4}$
0.01	$4.397838806966825 \cdot 10^{-3}$	$1.3460 \cdot 10^{-3}$
0.03	$2.219498738086498 \cdot 10^{-2}$	$3.7467 \cdot 10^{-3}$
0.1	$1.055162854697281 \cdot 10^{-1}$	$8.3746 \cdot 10^{-3}$
1.0	$1.801024605942818 \cdot 10^{-1}$	$1.1638 \cdot 10^{-2}$
2.0	$1.333459015123582 \cdot 10^{-1}$	$1.0673 \cdot 10^{-2}$
3.0	$1.053062819728655 \cdot 10^{-1}$	$9.9541 \cdot 10^{-3}$
5.0	$7.444629837254586 \cdot 10^{-2}$	$9.0068 \cdot 10^{-3}$
7.0	$5.780969662306304 \cdot 10^{-2}$	$8.3953 \cdot 10^{-3}$
10.0	$4.345906835580813 \cdot 10^{-2}$	$7.7775 \cdot 10^{-3}$

and the stress P_{xy}, are given in Table 11. The value of the exponent γ decreases monotonically as k increases. However, γ varies only slightly and it is rather close to 3.0; in fact it is bounded by $2.8 < \gamma < 3.3$. Also the approximation $\tilde{u}_4(y,k)$ does not cause much change to the L_2 global error $\|\delta u\|_2$, the half-channel total mass flow rate Q, and the stress P_{xy} when compared to $\tilde{u}_3(y,k)$. This indicates that the exponent γ has a very limited effect on the velocity $u(y,k)$ in terms of the L_2 global error $\|\delta u\|_2$, the half-channel total mass flow rate Q, and the stress P_{xy}, and $\tilde{u}_3(y,k)$ given by Eq. (28) with $\gamma = 3$ is a good approximation for the velocity $u(y,k)$.

In summary, the approximated solution $\tilde{u}_1(y,k)$ given by Eq. (24) in terms of Abramowitz functions captures the leading order singularities of $u(y,k)$ at the end-points, and approximates $u(y,k)$ very accurately. For many practical purposes, the approximation $\tilde{u}_2(y,k)$ of the cubic polynomial given by Eq. (27) can be used as an adequate model for wall-function.

3.4. The velocity defect and slip velocities

The linear velocity $u_1 := u'(0,k)y$ is the hydrodynamic component of the velocity $u(y,k)$. Thus, the kinetic component of the velocity $u(y,k)$ can be characterized by the so-called the "velocity defect" defined as the following [6]:

$$u_d(y,k) = \frac{\sqrt{2\pi}}{u(1/2,k)}[u(y,k) - u'(0,k)y]. \tag{30}$$

The velocity defect essentially shows the structure of Knudsen layer in the velocity profile $u(y,k)$. For Kramers' problem which has only one wall thus the flow domain is semi-infinite, *i.e.*, $0 \leqslant y < \infty$, the velocity defect is a function of y/k. For the Couette flow, the velocity defect $u_d(y,k)$ is *not* a function of y/k [6]. This can be seen clearly from the approximated solution of $u(y,k)$ given by Eqs. (22) and (23a): $u(y,k)$ is indeed a function of both y/k and k.

The microscopic slip velocity u_s and the macroscopic one U_s are defined as the following:

$$u_s(k) = U_w - u(1/2,k) = \frac{1}{2} - u(1/2,k), \tag{31}$$

$$U_s(k) = U_w - u'(0,k)y|_{y=1/2} = \frac{1}{2}[1 - u'(0,k)], \tag{32}$$

where $U_w := \pm U/2$ is the velocity of the wall at $y = \pm 1/2$ specified by the boundary conditions, and $u(1/2,k)$ and $u'(0,k)$ are the velocity at the wall and the velocity derivative at the channel center, respectively, obtained with the linearized BGK equation. Note that all the velocities are normalized by U. Clearly, the difference between U_s and u_s is due to the nonlinearity in $u(y,k)$ and can be used as a measure of that.

Fig. 4 shows the velocity defect $u_d(y,k)$ and the velocity defect $u_d(y,k)$ normalized by its maximum value at the boundary $u_d(1/2,k)$ for $k = 0.03$, 0.1, 1.0, and 10.0. The velocity defect $u_d(y,k)$ exhibits a non-monotonic dependence on k. First, $u_d(y,k)$ increases rapidly to its maximum at $k \approx 1$, then it decreases slightly and slowly as k further increases, as seen in the left figure in Fig. 4. The reason for this non-monotonic k-dependence of $u_d(y,k)$ is because of overlapping of the two Knudsen layers due to two walls, as clearly indicated by the leading order approximated solution of $u(y,k)$ given by Eq. (22), which includes terms singular at both walls. The non-monotonic dependence of the velocity defect $u_d(y,k)$ on k can be further quantified as the following. From Fig. 3 we can see that, as k increases, so does the slip velocity $u_s(k)$, hence the magnitude of the velocity $u(y,k)$ decreases. On the other hand, the kinetic component of the velocity, $u(y,k) - u'(0,k)y$, increases with k. That is, the nonlinearity in the velocity $u(y,k)$ increases while its magnitude $u(1/2,k)$ decreases as k increases. Therefore, the non-monotonic k dependence of the velocity defect $u_d(y,k)$ is due to the competition between the increasing nonlinearity and the decreasing magnitude of $u(1/2,k)$, which is characterized by the quantity $1 - u'(0,k)/2u(1/2,k)$. To make this point clearer, we show that the non-monotonic k-dependence of the velocity defect $u_d(y,k)$ can be removed when it is normalized by its maximum,

Table 9
The values $\tilde{u}_2(0,k)$, and the half-channel mass flow rate Q, and the stress P_{xy} computed from $\tilde{u}_2(y,k) = ay^3 + u'(0)y$.

k	$\tilde{u}_2(1/2)$	$Q(k)$	$P_{xy}(k)$
0.003	$4.970954621243941 \cdot 10^{-1} \pm 0.1599\%$	$1.242581703345339 \cdot 10^{-1} \pm 0.0110\%$	$-1.490909823701481 \cdot 10^{-3} \pm 1.2152 \cdot 10^{-10}$
0.01	$4.905902308048756 \cdot 10^{-1} \pm 0.5029\%$	$1.225788414698600 \cdot 10^{-1} \pm 0.0374\%$	$-4.900424799305580 \cdot 10^{-3} \pm 1.9789 \cdot 10^{-8}$
0.03	$4.740471733349583 \cdot 10^{-1} \pm 1.2414\%$	$1.181707716833412 \cdot 10^{-1} \pm 0.1322\%$	$-1.414048256521453 \cdot 10^{-2} \pm 2.4965 \cdot 10^{-6}$
0.1	$4.308324185072827 \cdot 10^{-1} \pm 2.3553\%$	$1.060594126663562 \cdot 10^{-1} \pm 0.3373\%$	$-4.165343452234106 \cdot 10^{-2} \pm 9.7356 \cdot 10^{-5}$
0.3	$3.563868803731906 \cdot 10^{-1} \pm 2.9481\%$	$8.601898986089533 \cdot 10^{-2} \pm 0.4882\%$	$-9.370544518610212 \cdot 10^{-2} \pm 2.5561 \cdot 10^{-4}$
1.0	$2.446270424475982 \cdot 10^{-1} \pm 2.8723\%$	$5.834265966511390 \cdot 10^{-2} \pm 0.5092\%$	$-1.696070068509743 \cdot 10^{-1} \pm 1.4443 \cdot 10^{-4}$
2.0	$1.804055261577246 \cdot 10^{-1} \pm 2.6132\%$	$4.301785182830057 \cdot 10^{-2} \pm 0.4700\%$	$-2.083977602271475 \cdot 10^{-1} \pm 6.5506 \cdot 10^{-5}$
3.0	$1.467667882167143 \cdot 10^{-1} \pm 2.4340\%$	$3.504628639835256 \cdot 10^{-2} \pm 0.4393\%$	$-2.266809875895623 \cdot 10^{-1} \pm 3.7237 \cdot 10^{-5}$
5.0	$1.101530032054535 \cdot 10^{-1} \pm 2.2037\%$	$2.649017400821707 \cdot 10^{-2} \pm 0.8365\%$	$-2.446801545148576 \cdot 10^{-1} \pm 1.6886 \cdot 10^{-5}$
7.0	$8.983052947568622 \cdot 10^{-2} \pm 2.0567\%$	$2.649017400821707 \cdot 10^{-2} \pm 0.8365\%$	$-2.537040133056390 \cdot 10^{-1} \pm 9.6593 \cdot 10^{-6}$
10.0	$7.153017307032454 \cdot 10^{-2} \pm 1.9088\%$	$1.720349532452163 \cdot 10^{-2} \pm 0.3442\%$	$-2.611676684381582 \cdot 10^{-1} \pm 5.2080 \cdot 10^{-6}$

Table 10
The L_2 global error of the approximated solution $\tilde{u}_3(y,k) = 4[2u(1/2,k) - u'(0,k)]y^3 + u'(0,k)y$, the half-channel total mass flow rate Q, and the stress P_{xy}.

k	$\|\delta u\|_2$	$Q(k)$	$P_{xy}(k)$
0.003	$1.1469 \cdot 10^{-3}$	$1.243576794787881 \cdot 10^{-1} \pm 0.0910\%$	$-1.490910597484586 \cdot 10^{-3} \pm 8.9531 \cdot 10^{-10}$
0.01	$3.6347 \cdot 10^{-3}$	$1.228887852159983 \cdot 10^{-1} \pm 0.2903\%$	$-4.900514063030057 \cdot 10^{-3} \pm 1.0905 \cdot 10^{-7}$
0.03	$9.2130 \cdot 10^{-3}$	$1.189098335236083 \cdot 10^{-1} \pm 0.7585\%$	$-1.414617804249189 \cdot 10^{-2} \pm 8.1920 \cdot 10^{-6}$
0.1	$1.8350 \cdot 10^{-2}$	$1.073584404744730 \cdot 10^{-1} \pm 1.5663\%$	$-4.183060986138169 \cdot 10^{-2} \pm 2.7453 \cdot 10^{-4}$
0.3	$2.3822 \cdot 10^{-2}$	$8.737220100800198 \cdot 10^{-2} \pm 2.0690\%$	$-9.425838992151225 \cdot 10^{-2} \pm 8.0855 \cdot 10^{-4}$
1.0	$2.3595 \cdot 10^{-2}$	$5.924694685784809 \cdot 10^{-2} \pm 2.0670\%$	$-1.699706480158879 \cdot 10^{-1} \pm 5.0807 \cdot 10^{-4}$
2.0	$2.1464 \cdot 10^{-2}$	$4.362294848033766 \cdot 10^{-2} \pm 1.8833\%$	$-2.085717852369104 \cdot 10^{-1} \pm 2.3953 \cdot 10^{-4}$
3.0	$1.9953 \cdot 10^{-2}$	$3.550396843366418 \cdot 10^{-2} \pm 1.7510\%$	$-2.267821881356465 \cdot 10^{-1} \pm 1.3843 \cdot 10^{-4}$
5.0	$1.8000 \cdot 10^{-2}$	$2.668530049229303 \cdot 10^{-2} \pm 1.5793\%$	$-2.447270513741618 \cdot 10^{-1} \pm 6.3783 \cdot 10^{-5}$
7.0	$1.6753 \cdot 10^{-2}$	$2.179015169162721 \cdot 10^{-2} \pm 1.4694\%$	$-2.537311316853772 \cdot 10^{-1} \pm 3.6777 \cdot 10^{-5}$
10.0	$1.5501 \cdot 10^{-2}$	$1.737748781489167 \cdot 10^{-2} \pm 1.3590\%$	$-2.611824247306578 \cdot 10^{-1} \pm 1.9964 \cdot 10^{-5}$

Table 11
The exponent γ, the L_2 global error, the mass flow rate Q, and the stress P_{xy} computed by using $\tilde{u}_4(y,k)$ of Eq. (29).

k	γ	$\|\delta u\|_2$	$Q(k)$	$P_{xy}(k)$
0.003	3.248329323033803	$1.1050 \cdot 10^{-3}$	$1.243509453925648 \cdot 10^{-1} \pm 0.0856\%$	$-1.490910081133585 \cdot 10^{-3} \pm 3.7896 \cdot 10^{-10}$
0.01	3.239676061098960	$3.4945 \cdot 10^{-3}$	$1.228673789267926 \cdot 10^{-1} \pm 0.2729\%$	$-4.900468505233785 \cdot 10^{-3} \pm 6.3495 \cdot 10^{-8}$
0.03	3.187314282375971	$8.8572 \cdot 10^{-3}$	$1.188610006583377 \cdot 10^{-1} \pm 0.7171\%$	$-1.414450517167787 \cdot 10^{-2} \pm 6.5191 \cdot 10^{-6}$
0.1	3.031991051258164	$1.8150 \cdot 10^{-2}$	$1.073350523634845 \cdot 10^{-1} \pm 1.5442\%$	$-4.182382594026332 \cdot 10^{-2} \pm 2.6774 \cdot 10^{-4}$
0.3	2.916177429820853	$2.4838 \cdot 10^{-2}$	$8.746704167888562 \cdot 10^{-2} \pm 2.1798\%$	$-9.431350942302831 \cdot 10^{-2} \pm 8.6367 \cdot 10^{-4}$
1.0	2.855100787910733	$2.5821 \cdot 10^{-2}$	$5.938670753890424 \cdot 10^{-2} \pm 2.3078\%$	$-1.700359908390864 \cdot 10^{-1} \pm 5.7341 \cdot 10^{-4}$
2.0	2.836174755461950	$2.3952 \cdot 10^{-2}$	$4.373776725150815 \cdot 10^{-2} \pm 2.1514\%$	$-2.086079889573638 \cdot 10^{-1} \pm 2.7573 \cdot 10^{-4}$
3.0	2.828237564262746	$2.2466 \cdot 10^{-2}$	$3.559832838838151 \cdot 10^{-2} \pm 2.0214\%$	$-2.268045365488366 \cdot 10^{-1} \pm 1.6078 \cdot 10^{-4}$
5.0	2.820598517515874	$2.0453 \cdot 10^{-2}$	$2.675449055715516 \cdot 10^{-2} \pm 1.8426\%$	$-2.447380163789222 \cdot 10^{-1} \pm 7.4748 \cdot 10^{-5}$
7.0	2.816697371284773	$1.9129 \cdot 10^{-2}$	$2.184485735317340 \cdot 10^{-2} \pm 1.7241\%$	$-2.537376600108247 \cdot 10^{-1} \pm 4.3306 \cdot 10^{-5}$
10.0	2.813344241739956	$1.7776 \cdot 10^{-2}$	$1.741924247925830 \cdot 10^{-2} \pm 1.6026\%$	$-2.611860675848703 \cdot 10^{-1} \pm 2.3607 \cdot 10^{-5}$

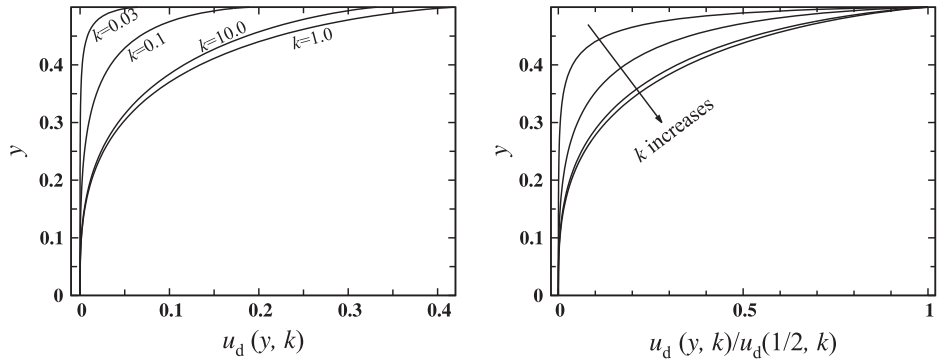

Fig. 4. The velocity defect $u_d(y,k)$ (left) and the normalized velocity defect $u_d(y,k)/u_d(1/2,k)$ (right) for $k = 0.03$, 0.1, 1.0, and 10.0. Note that the normalized velocity defect $u_d(y,k)/u_d(1/2,k)$ (right) increases monotonically as k increases.

$u_d(1/2,k)$ that is, $u_d(y,k)/u_d(1/2,k)$ increases with k monotonically, as shown in the right figure in Fig. 4.

The microscopic slip velocity $u_s(k)$ can be directly extracted from the accurate data of the $u(y,k)$ given in the previous section. To gain some insights of the Knudsen number dependence of $u_s(k)$, we can use the approximated solutions of $u(y,k)$ discussed previously. To capture the singular behavior of $u(y,k)$, we have to use $\tilde{u}_1(y,k)$ of Eq. (24) given in terms of Abramowitz functions I_0 and I_1. Similarly, we can approximate $u_s(k)$ in terms of I_0 and I_1 with the following formula:

$$u_{s1}(k) = \frac{k}{1+2A_2k}\left[A_2 + A_0\left(I_0(1/k) - \frac{\sqrt{\pi}}{2}\right) + A_1\left(I_1(1/k) - \frac{1}{2}\right)\right], \tag{33}$$

where coefficients A_0, A_1, and A_2, are obtained by the least-square fitting of $u_s(k)$ with $0.003 \leqslant k \leqslant 10.0$. The data of $u_s(k) := 1/2 - u(1/2,k)$ are extracted from the data of $u(1/2,k)$ given in Table 4. The above approximation of $u_s(k)$ includes the correct asymptotic behaviors of $u_s(k)$, *i.e.*, $u_s(0) = 0$ and $u_s(k) \to 1/2$ as $k \to \infty$.

In consideration of the limits of $u_s(k)$ at $k = 0$ and at infinity, we can use the following simple approximation for $u_s(k)$:

$$u_{s2}(k) = \frac{B_1k + B_2\ln(1+k)}{1+2B_1k}, \tag{34}$$

where parameters B_1 and B_2 are obtained by the least-square fitting in the interval $0.003 \leqslant k \leqslant 0.3$. To maintain the correct limits at $k = 0$ and at infinity, we can use a much simpler rational approximation of $u_s(k)$:

$$u_{s3}(k) = \frac{C_1k}{1+C_2k}, \tag{35}$$

where coefficients C_1 and C_2 are obtained by the least-square fitting in the interval $0.003 \leqslant k \leqslant 0.3$. We can set $C_2 = 2C_1$ to satisfy the asymptotic limit of $u_s(k)$ at $k \to \infty$. However, this increases the L_2 error in the fitting range of k.

Finally, we can also use the following cubic polynomial to approximate $u_s(k)$ for $k < 1$:

$$u_{s3}(k) = D_1k + D_2k^2 + D_3k^3, \tag{36}$$

where coefficients D_1, D_2, and D_3 are obtained by the least-square fitting for $0.003 \leqslant k \leqslant 0.3$. The values of the parameters in models u_{s1}, u_{s2}, u_{s3}, and u_{s4}, given by Eqs. (33)–(36), respectively, as well as the L_2 error of the models in the range of k in which the parameters are obtained, are given in Table 12.

Fig. 5 shows the Knudsen number dependence of the slip velocity $u_s(k)$ as well as the approximations of $u_s(k)$ given by Eqs. (33)–(36). Clearly, the model of Eq. (33) approximates $u_s(k)$ very well, the asymptotic values of $u_s(k)$ in both $k = 0$ and $k \to \infty$ are matched by Eq. (33) exactly, and the L_2 global error is $1.1205 \cdot 10^{-3}$ in the range of $0.003 \leqslant k \leqslant 10.0$. Although the parameters B_1 and B_2 in Eq. (34) are obtained in the interval $0.003 \leqslant k \leqslant 0.3$, the model of Eq. (34) is indistinguishable from that of Eq. (33). The models of Eqs. (35) and (36) are only valid for small k in the interval $0.003 \leqslant k \leqslant 0.3$ – the L_2 global errors of these models are $5.0112 \cdot 10^{-4}$ and $9.4363 \cdot 10^{-5}$, respectively. Note that while the model of Eq. (35) with $C_2 = 2C_1$ has the correct asymptotic limits at both $k = 0$ and $k \to \infty$, the model with $C_2 \neq 2C_1$ actually fits $u_s(k)$ better in the interval $0.003 \leqslant k \leqslant 0.3$.

When considering slip-velocity models which can be used as boundary conditions in the Navier–Stokes equations, the macroscopic slip velocity $U_s(k)$ is used [56,52]. The models for $U_s(k)$ can be directly derived from those for the velocity $u(y,k)$. Since the models for $U_s(k)$ are only useful for small k, we will only consider the following cubic polynomial approximation of $U_s(k)$:

Table 12
The values of parameters in the models for the (microscopic) slip velocity $u_s(k)$, the fitting range of k for the parameters, and the L_2 of the models in the corresponding fitting range of k.

Model	Parameters	k range	$\|\delta u_s\|_2$
Eq. (33)	$A_0 = 0.4701623488541722$ $A_1 = -0.3569325916063242$ $A_2 = 0.9303088949385295$	$0.003 \leqslant k \leqslant 10.0$	$1.1205 \cdot 10^{-3}$
Eq. (34)	$B_1 = 1.279758697826314$ $B_2 = -0.5685759260098272$	$0.003 \leqslant k \leqslant 0.3$	$4.6599 \cdot 10^{-4}$
Eq. (35)	$C_1 = 0.7037931880441636$ $C_2 = 1.967040348835866$	$0.003 \leqslant k \leqslant 0.3$	$5.0112 \cdot 10^{-4}$
Eq. (35)	$C_1 = 0.6171898550504058$ $C_2 = 2C_1$	$0.003 \leqslant k \leqslant 0.3$	$3.4415 \cdot 10^{-2}$
Eq. (36)	$D_1 = 0.7049600580160285$ $D_2 = -1.320955381122892$ $D_3 = 1.488348609420158$	$0.003 \leqslant k \leqslant 0.3$	$9.4363 \cdot 10^{-5}$

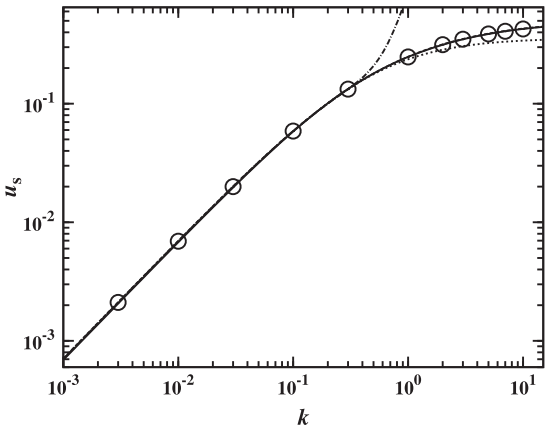

Fig. 5. The k-dependence of the slip velocity $u_s(k)$. The circles are the solution of the integral Eq. (2a) given in Table 4. The solid, dash, dot, and dash-dot lines are the approximations of $u_s(k)$ by Eqs. (33), (34), (35) with $C_2 \neq 2C_1$, and (36), respectively. Note that the lines of Eqs. (33) and (34) overlap each other completely.

$$U_s(k) \approx \overline{C}_1k + \overline{C}_2k^2 + \overline{C}_3k^3, \tag{37}$$

where $\overline{C}_1 = 1.020794919617355$, $\overline{C}_2 = -2.191441518439700$, and $\overline{C}_3 = 2.193562264423130$, and the L_2 error is $1.9880 \cdot 10^{-4}$ for $0.003 \leqslant k \leqslant 0.3$. In Fig. 6 we show $U_s(k)$ directly computed from the solution of the integral Eq. (2a), the model derived from Eq. (24) and the cubic polynomial fit of Eq. (37). Clearly, the cubic polynomial fit of Eq. (37) approximates $U_s(k)$ adequately for $k \leqslant 0.3$. In fact, the cubic polynomial fitting (37) approximate $U_s(k)$ better than the model derived from Eq. (33) does for $k \leqslant 0.3$.

The half channel mass flow rate $Q(k)$ is a measure of not only the effect due to the slip velocity $u_s(y)$, but also the structure of the Knudsen layer in the velocity profile $u(y,k)$ [24]. Based on the approximation of $u(y,k)$ given by Eq. (33), we can approximate $Q(k)$ with the following formula:

$$Q_1(k) = \frac{k}{1+\overline{A}_3k}\left[\frac{1}{8k} + \overline{A}_1k\left(\frac{1}{2} + I_1(1/k) - 2I_1(1/2k)\right) + \overline{A}_2k\left(\frac{\sqrt{\pi}}{4} + I_2(1/k) - 2I_2(1/2k)\right)\right], \tag{38}$$

where $\overline{A}_1, \overline{A}_2$, and $\overline{A}_3$ are obtained range $0.003 \leqslant k \leqslant 10.0$. A simpler approximation of $Q(k)$ is:

$$Q_2(k) = \frac{1 + 8\overline{B}_1\ln\left(1+k^2\right)}{1+\overline{B}_2k}, \tag{39}$$

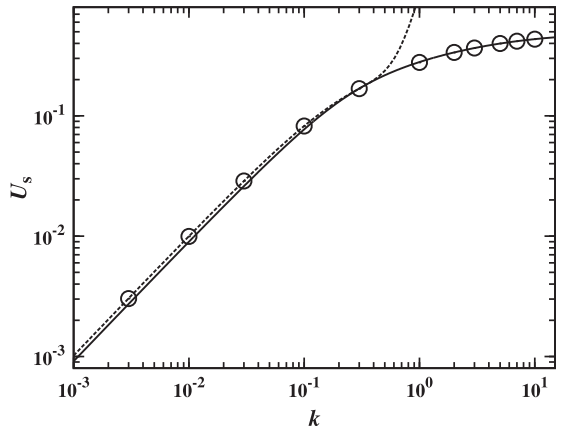

Fig. 6. The k-dependence of the macro-slip velocity $U_s(k)$. The circles are the solution of the integral Eq. (2a). The solid and dash lines are the approximations of $U_s(k)$ by the model derived from Eq. (24) and the cubic polynomial fit given by Eq. (37), respectively.

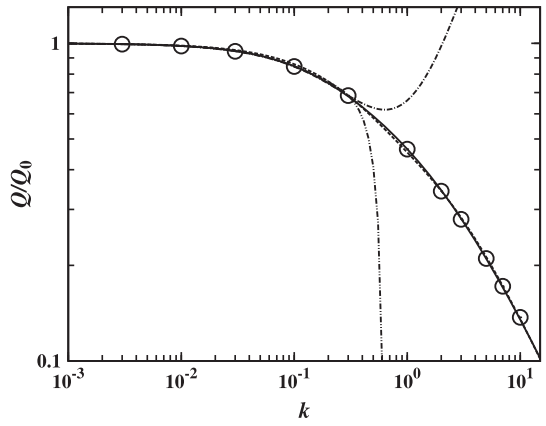

Fig. 7. The k-dependence of the normalized half-channel mass flow rate $Q(k)/Q_0$. The circles are the solution of the integral Eq. (2a) given in Table 4. The solid, dash, dash-dot, and dash-dot-dot lines are the approximations of $Q(k)/Q_0$ by Eqs. (38), (39), (41), and (42) respectively. Note that the lines for Eqs. (38) and (39) are overlapped with each other.

where $\overline{B}_1$ and $\overline{B}_2$ are also obtained by the least-square fitting for $0.003 \leqslant k \leqslant 10.0$. We note that both $Q_1(k)$ and $Q_2(k)$ have the correct behaviors in both $k = 0$ and $k \to \infty$, *i.e.*, $Q(0) = 1/8$ and

$$\lim_{k\to\infty} Q(k) = 0. \tag{40}$$

For small $k < 1$, we can use the following rational approximation

$$Q_3(k) = \frac{1 + 8\overline{C}_1 k^2}{8(1 + \overline{C}_2 k)}, \tag{41}$$

where $\overline{C}_1$ and $\overline{C}_2$ are obtained for $0.003 \leqslant k \leqslant 0.3$. We can also use a cubic polynomial to fit $Q(k)$:

$$Q_4(k) = \frac{1}{8} + \overline{D}_1 k + \overline{D}_2 k^2 + \overline{D}_3 k^3, \tag{42}$$

where $\overline{D}_1, \overline{D}_2$, and $\overline{D}_3$ are also obtained for $0.003 \leqslant k \leqslant 0.3$. The values of the parameters in the models for $Q(k)$ are given in Table 13.

Fig. 7 shows the half-channel mass flow rate $Q(k)$ normalized its value at $k = 0$, *i.e.*, $Q_0 = 1/8$, as well as the models for $Q(k)$ given by Eqs. (38), (39), (41), and (42). Clearly, the approximation of Eq. (38) with Abramowitz functions I_1 and I_2 covers the entire range of k with the correct limits at both $k = 0$ and ∞ and it quantitatively agrees with the solution of the integral Eq. (2a). It is interesting to note that, although the simple analytic model of Eq. (39) uses only elementary functions with two fitting parameters, it also has the correct limits at $k = 0$ and ∞, and approximates $Q(k)$ quite accurately, as indicated by its small L_2 error. It is also interesting to note that the cubic polynomial of Eq. (42) is a very accurate approximation of $Q(k)$ for small values of k, *i.e.*, $k \leqslant 0.3$.

Table 13
The values of parameters in the models for the half-channel flow rate $Q(k)$, the fitting range of k for the parameters, and the L_2 errors of the models in the corresponding fitting range of k.

Model	Parameters	k range	$\|\delta Q\|_2$
Eq. (38)	$\overline{A}_1 = 0.4339896731456645$ $\overline{A}_2 = -0.2037173094079779$ $\overline{A}_3 = 1.916439270306587$	$0.003 \leqslant k \leqslant 10.0$	$2.7451 \cdot 10^{-3}$
Eq. (39)	$\overline{B}_1 = 0.03771029254176309$ $\overline{B}_2 = 1.665037574894380$	$0.003 \leqslant k \leqslant 10.0$	$9.6796 \cdot 10^{-3}$
Eq. (41)	$\overline{C}_1 = 0.1187836129667822$ $\overline{C}_2 = 1.949726554024494$	$0.003 \leqslant k \leqslant 0.3$	$9.0564 \cdot 10^{-4}$
Eq. (42)	$\overline{D}_1 = -0.2529994267391535$ $\overline{D}_2 = 0.6976773399315172$ $\overline{D}_3 = -0.9737045663563917$	$0.003 \leqslant k \leqslant 0.3$	$2.8209 \cdot 10^{-5}$

4. Conclusion

In this work, we present an accurate and efficient high-order method to solve the integral equation derived from linearized BGK equation. The numerical technique used in this work differs from the previous approaches in two aspects. First, the method used in this work is based on a collocation method, as opposed to the quadrature method or the Nyström method. And second, the singular integral kernels are represented in terms of Chebyshev expansion, as opposed to the Meijer G-function. The high-order collocation method and Chebyshev expansion enable us to solve the integral equation with high precision for the steady Couette flow in a wide range of the Knudsen number $0.003 \leqslant k \leqslant 10.0$, which covers from near-continuum to free-molecular flow region. We compute the velocity $u(y,k)$, the stress $P_{xy}(k)$, and the half-channel mass flow rate $Q(k)$. We also compute the slip velocity and the velocity defect. With mostly double-precision arithmetic and a linear system no larger than 2048×2048, we can obtain results correct to at least eleven (11) significant digits in a wide range of the Knudsen number $0.003 \leqslant k \leqslant 10.0$. Our results are much more accurate than the existing ones, and are perhaps the most accurate ones available to date thus can be used as benchmark data.

Using the accurate data obtained in this work, we also consider various approximations for the velocity $u(y,k)$, the slip velocities $u_s(k)$ and $U_s(k)$, and the half-channel flow rate $Q(k)$. These approximations can be useful for modeling and simulation of Couette flow in a wide range of the Knudsen number.

It should be emphasized that the present method is effective and efficient to solve the integral equation derived from the linearized BGK equation. While we have only dealt with the isothermal Couette flow in this work, we would like to point out that integral equations for both the velocity and temperature can also be derived from the linearized BGK equation [57–59], to which our method can be directly applied. Of course, there exist other deterministic methods to solve the kinetic equation, such as discrete ordinates methods [20,60,61], discrete velocity models [62,63], and gas kinetic scheme [64,65]. However, to our best knowledge, none of these methods can yield results of benchmark quality with very high precision as the present method.

We note that the Chebyshev expansion method appears to have two limitations. First, it cannot *directly* deal with the singularities

of the velocity at the boundaries, that is, the Chebyshev expansion cannot be used to accurately compute $u'(y,k)$ when y is very close to the boundaries and $|u'(y,k)| \to \infty$. And second, the Chebyshev expansion of the Abramowitz functions appears to be valid only for real argument. Thus it is not suitable for problems which require the Abramowitz functions with complex argument, such as Stokes' second problem. Our future work will be to apply our method for other canonical flows in kinetic theory.

Acknowledgments

WL and LSL would like to thank Profs. John Tweed at Old Dominion University (ODU) and Prof. Allan MacLeod at University of The West Scotland, UK, for helpful discussions on collocation methods for integral equations and Chebyshev expansion method, respectively. We are also grateful to Prof. Richard Noren at ODU for his carefully reading of our manuscript and comments. WL would like to acknowledge the generous support of the Modeling and Simulation Scholarship provided by ODU. LSL would like to acknowledge the support of the Richard F. Barry Jr. endowment at ODU and a visiting fellowship from the Isaac Newton Institute of Mathematical Sciences, Cambridge, UK, July 6 – August 3, 2013, during which part of this work was done. This work is supported by the National Science Foundation (NSF) of the United States through Grant DMS-0807983 (LSL) and National Science Foundation of China (NSFC) through Grants 91130002 and 11371298 (JS).

Appendix A. Properties and approximations of Abramowitz functions I_n

In this section we provide a succinct summary of some useful properties of Abramowitz functions $I_n(x)$ and the approximation formulas to evaluate $I_n(x)$, which can be found in the work of MacLeod [41] and Handbook of Mathematical Functions edited by Abramowitz and Stegun [66].

Abramowitz functions satisfy the following differential equation and recurrence relations:

$$xI_n''' - (n-1)I_n'' + 2I_n = 0, \tag{A.1a}$$

$$I_{n+1}' + I_n = 0, \tag{A.1b}$$

$$2I_n = (n-1)I_{n-2} + xI_{n-3}. \tag{A.1c}$$

The first-order Abramowitz function I_1 has the following expansion:

$$I_1(x) = \sum_{k=0}^{\infty}(a_k \ln x + b_k)x^k, \tag{A.2}$$

with $a_0 = a_1 = 0$, $a_2 = -1$, $b_0 = 1$, $b_1 = \sqrt{\pi}$, $b_2 = 3(1-\gamma)/2$, where γ is Euler's constant, and for $k \geqslant 3$:

$$a_k = -\frac{2a_{k-2}}{k(k-1)(k-2)}, \quad b_k = -\frac{2b_{k-2} + (3k^2 - 6k + 2)a_k}{k(k-1)(k-2)}. \tag{A.3}$$

In particular, we have

$$\begin{aligned} I_1(x) = {} & \frac{1}{2} + \frac{3}{4}(1-\gamma)x^2 + \frac{1}{188}(18\gamma - 3)x^4 + \cdots \\ & - \sqrt{\pi}x\left(\frac{1}{2} - \frac{1}{6}x^2 + \frac{1}{180}x^4 - \cdots\right) - x^2 \\ & \times \ln x\left(\frac{1}{2} - \frac{1}{24}x^2 + \frac{1}{1440}x^4 - \cdots\right). \end{aligned} \tag{A.4}$$

Also, I_n can be approximated by the following asymptotic formulas:

$$I_n(x) \sim \begin{cases} \pi^{(1-\sigma)/2} f_n(x) - \pi^{\sigma/2} x g_n(x) + (-1)^n h_n(x) x^{n+1} \ln x, & 0 \leqslant x \leqslant 2, \\ \sqrt{\pi/3}(v/3)^{n/2} e^{-v} q_n(v), & x > 2, \end{cases} \tag{A.5}$$

where $v := 2(x/2)^{2/3}$, $\sigma := ||(n+1)/2\rfloor - \lfloor n/2\rfloor|$ and $\lfloor x\rfloor$ is the integer part of x, *i.e.*, $\sigma = 1$ for $n = (2k+1)$, and $\sigma = 0$ for $n = 2k$ or $n = 0$; and $f_n(x)$, $g_n(x)$, $h_n(x)$, and $q_n(v)$ are analytic functions which can be accurately given by their Chebyshev expansions [41].

To solve the integral Eq. (1a) or (2a), we need to compute $I_{-1}(x)$ and $I_0(x)$ according to the procedure of MacLeod [41]. First, $I_0(x), I_1(x)$, and $I_2(x)$ are computed by the asymptotic formulas (A.5). Then $I_{-1}(x)$ is computed in three intervals. In the first interval $0 < x \leqslant \varepsilon$, we use the following formula:

$$I_{-1}(x) = I_1''(x), \tag{A.6}$$

which is derived from Eq. (A.1b). For $x > \varepsilon$, we use the following formula:

$$I_{-1}(x) = \frac{2I_2(x) - I_0(x)}{x}, \tag{A.7}$$

where both $I_0(x)$ and $I_2(x)$ are given by the first and second asymptotic formula in Eq. (A.5) for the second interval $\varepsilon < x \leqslant 2.0$ and the third one $x > 2.0$, respectively. Finally, $I_{-1}(x)$ is computed with the following formulas:

$$I_{-1}(x) \sim \begin{cases} -\frac{3\gamma}{2} + \sqrt{\pi}x + \left(\frac{54}{47}\gamma - \frac{1903}{1128}\right)x^2 - \left(1 - \frac{x^2}{2}\right)\ln x, & 0 < x \leqslant \varepsilon, \\ \frac{\sqrt{\pi}[2f_2(x) - f_0(x)]}{x} - [2g_2(x) - g_0(x)] & \\ \quad + \left[2x^2 h_2(x) - h_0(x)\right]\ln x, & \varepsilon < x \leqslant 2.0, \\ \sqrt{\frac{\pi}{3}}e^{-v}\left[\frac{2v}{3}q_2(v) - q_0(v)\right], & 2.0 < x, \end{cases} \tag{A.8}$$

where $v := 2(x/2)^{2/3}$ and $\varepsilon = 1.5 \cdot 10^{-8}$.

Appendix B. Nonexistence of $u'(y,k)$ at the boundaries $y = \pm 1/2$

We prove that the velocity derivative $u'(y,k)$ does not exist at the boundaries, *i.e.*,

$$\lim_{y \to \pm 1/2} u'(y,k) \to \pm\infty. \tag{B.1}$$

Differentiation of Eq. (1a) leads to the following equation:

$$u'(y,k) - \frac{1}{k\sqrt{\pi}}\int_{-1/2}^{1/2}\frac{\mathrm{d}}{\mathrm{d}y}I_{-1}\left(\frac{|y-s|}{k}\right)u(s)\mathrm{d}s = \frac{1}{2k\sqrt{\pi}}G_{-1}(y,k). \tag{B.2}$$

Because

$$\begin{aligned} \int_{-1/2}^{1/2} u(s)\frac{\mathrm{d}}{\mathrm{d}y}I_{-1}\left(\frac{|y-s|}{k}\right)\mathrm{d}s &= -\int_{-1/2}^{1/2} u(s)\frac{\mathrm{d}}{\mathrm{d}s}I_{-1}\left(\frac{|y-s|}{k}\right)\mathrm{d}s \\ &= -G_{-1}(y,k)u(1/2) + \int_{-1/2}^{1/2} I_{-1}\left(\frac{|y-s|}{k}\right)u'(s)\mathrm{d}s, \end{aligned}$$

then Eq. (B.2) becomes

$$u'(y,k) - \frac{1}{k\sqrt{\pi}}\int_{-1/2}^{1/2} I_{-1}\left(\frac{|y-s|}{k}\right)u'(s)\mathrm{d}s = \frac{1-2u(1/2)}{2k\sqrt{\pi}}G_{-1}(y,k). \tag{B.3}$$

With $y = 1/2$, Eq. (B.3) leads to

$$\begin{aligned} u'(1/2,k) = {} & \frac{[1-2u(1/2)]}{2k\sqrt{\pi}}[I_{-1}(0) - I_{-1}(1/k)] + \frac{1}{k\sqrt{\pi}} \\ & \times \int_{-1/2}^{1/2} I_{-1}\left(\frac{1-2s}{2k}\right)u'(s)\mathrm{d}s. \end{aligned}$$

It can be shown that $u(y,k) < 1/2$ for $k > 0$ and $u'(y,k) > 0$, therefore the above equation leads to the conclusion that $u'(1/2,k)$ does not exist for $k > 0$, because $I_{-1}(0)$ does not exist due to its logarithmic singularity at $x = 0$ [cf. Eqs. (A.5) and (A.8)].

Appendix C. Evaluation of integrals involving I_{-1} and T_n

To solve the integral Eq. (2a), we need to evaluate the following integral accurately:

$$\Psi_j(x,k) := \int_{-1}^{1} I_{-1}\left(\frac{|x-s|}{2k}\right)[T_{2j+1}(s) - T_{2j+1}(x)]\mathrm{d}s. \tag{C.1}$$

With the following collocation points,

$$x_{2i+1} = \begin{cases} 1, & i = 0, \\ \cos\theta_i, & i = 1,2,\ldots,N, \end{cases} \tag{C.2}$$

where $\theta_i := (4i-1)\pi/4N$, the integral (C.1) becomes

$$\Psi_{ij}(k) := \int_0^{\pi} K_{ij}(\theta,k)\mathrm{d}\theta, \tag{C.3}$$

$$K_{ij}(\theta,k) := I_{-1}\left(\frac{|\cos\theta - \cos\theta_i|}{2k}\right)[\cos(2j+1)\theta - \cos(2j+1)\theta_i]\sin\theta. \tag{C.4}$$

The integrand $K_{ij}(\theta,k)$ is highly oscillatory when $j \gg 1$ and becomes singular at collocation points x_{2i+1} because $I_{-1}(x)$ has a $\ln x$ singularity at $x = 0$ [cf. Eq. (A.5)]. To address the numerical difficulties caused by oscillatory and singular behaviors of the integrand, we divide the interval of integration, $[0,\pi]$, into $2(j+1)$ sub-intervals, for $1 \leqslant j \leqslant N$, such that two adjacent sub-intervals, excluding two sub-intervals at two ends, cover exactly one period of $\cos(2j+1)\theta$ so the integrand in the sub-intervals are slow varying. Also, the singularity of $I_{-1}(x)$ occurs at $\cos\theta = \cos\theta_i$, which is an end-point of two sub-intervals. Because the abscissas of the generalized Gaussian quadrature do not include the end points, this mitigates the difficulty caused by the singularity.

The interval $[0,\pi]$ has to be divided in two ways depending on both i and j. Denote l^* and r as the integer part and the remainder of $(4i-1)(2j+1)/4N$, *i.e.*,

$$l^* := \left\lfloor \frac{(4i-1)(2j+1)}{4N} \right\rfloor, \quad r := \frac{(4i-1)(2j+1)}{4N} - l^*, \tag{C.5}$$

where $i = 1,2,\ldots,N$, and $j = 0,1,\ldots,N$. We further introduce the following notations:

$$\bar{r} := 1 - r, \quad \varphi_j := \frac{\pi}{2j+1}. \tag{C.6}$$

For even and odd l^*, the interval $[0,\pi]$ is divided into $2(j+1)$ sub-intervals as follows:

$$[0,\pi] = [0, r\varphi_j] + \bigcup_{l=0}^{j-1}\{[l_1 - \bar{r}, l_1 + \bar{r}] + [l_2 - r, l_2 + r]\}\varphi_j + [\pi - \bar{r}\varphi_j, \pi], \quad l^* \text{ even},$$

$$[0,\pi] = [0, \bar{r}\varphi_j] + \bigcup_{l=0}^{j-1}\{[l_1 - r, l_1 + r] + [l_2 - \bar{r}, l_2 + \bar{r}]\}\varphi_j + [\pi - r\varphi_j, \pi], \quad l^* \text{ odd},$$

where $l_1 := 2l+1$ and $l_2 := 2(l+1)$. The interval $[l_1 - \bar{r}, l_1 + \bar{r}]\varphi_j$ has the end-points $(2l+1\pm\bar{r})\varphi_j$, and $[l_2 - r, l_2 + r]\varphi_j$ has the end-points $(2l+2\pm r)\varphi_j$. Clearly, in the above divisions any two adjacent sub-intervals, excluding two sub-intervals at two ends, cover $2\varphi_j = 2\pi/(2j+1)$ for $0 \leqslant j \leqslant N$, which is exactly one period of $\cos(2j+1)\theta$ for $\theta \in [0,2\pi]$.

For even l^*, the integrals on the sub-intervals are:

$$\int_0^{r\varphi_j} K_{ij}(\theta,k)\mathrm{d}\theta = r\varphi_j \int_{-1}^{1} I_{-1}\left(\frac{1}{k}\left|\sin\left[\frac{(1+s)r\varphi_j}{4} + \frac{\theta_i}{2}\right]\right.\right. \left.\left.\sin\left[\frac{(1+s)r\varphi_j}{4} - \frac{\theta_i}{2}\right]\right|\right) \sin\frac{(3+s)r\pi}{4}\sin\frac{(1-s)r\pi}{4} \sin\left[\frac{(1+s)r\varphi_j}{2}\right]\mathrm{d}s, \tag{C.7a}$$

$$\int_{(l_1-\bar{r})\varphi_j}^{(l_1+\bar{r})\varphi_j} K_{ij}(\theta,k)\mathrm{d}\theta = -2\bar{r}\varphi_j \int_{-1}^{1} I_{-1}\left(\frac{1}{k}\left|\sin\left[\frac{(l_1+\bar{r}s)\varphi_j}{2} + \frac{\theta_i}{2}\right]\right.\right. \left.\left.\sin\left[\frac{(l_1+\bar{r}s)\varphi_j}{2} - \frac{\theta_i}{2}\right]\right|\right) \sin\frac{(1+s)\bar{r}\pi}{2}\sin\frac{(1-s)\bar{r}\pi}{2} \sin[(l_1+\bar{r}s)\varphi_j]\mathrm{d}s, \tag{C.7b}$$

$$\int_{(l_2-r)\varphi_j}^{(l_2+r)\varphi_j} K_{ij}(\theta,k)\mathrm{d}\theta = 2r\varphi_j \int_{-1}^{1} I_{-1}\left(\frac{1}{k}\left|\sin\left[\frac{(l_2+rs)\varphi_j}{2} + \frac{\theta_i}{2}\right]\right.\right. \left.\left.\sin\left[\frac{(l_2+rs)\varphi_j}{2} - \frac{\theta_i}{2}\right]\right|\right) \sin\frac{(1+s)r\pi}{2}\sin\frac{(1-s)r\pi}{2} \sin\left[(l_2+rs)\varphi_j\right]\mathrm{d}s, \tag{C.7c}$$

$$\int_{\pi-\bar{r}\varphi_j}^{\pi} K_{ij}(\theta,k)\mathrm{d}\theta = -\bar{r}\varphi_j \int_{-1}^{1} I_{-1}\left(\frac{1}{k}\left|\cos\left[\frac{(1-s)\bar{r}\varphi_j}{4} + \frac{\theta_i}{2}\right]\right.\right. \left.\left.\cos\left[\frac{(1-s)\bar{r}\varphi_j}{4} - \frac{\theta_i}{2}\right]\right|\right) \sin\frac{(1+s)\bar{r}\pi}{4}\sin\frac{(3-s)\bar{r}\pi}{4} \sin\frac{(1-s)\bar{r}\varphi_j}{2}\mathrm{d}s. \tag{C.7d}$$

Similarly, for odd l^*, the integrals on the sub-intervals are:

$$\int_0^{\bar{r}\varphi_j} K_{ij}(\theta,k)\mathrm{d}\theta = \bar{r}\varphi_j \int_{-1}^{1} I_{-1}\left(\frac{1}{k}\left|\sin\left[\frac{(1+s)\bar{r}\varphi_j}{4} + \frac{\theta_i}{2}\right]\sin\left[\frac{(1+s)\bar{r}\varphi_j}{4} - \frac{\theta_i}{2}\right]\right|\right) \sin\frac{(3+s)\bar{r}\pi}{4}\sin\frac{(1-s)\bar{r}\pi}{4}\sin\frac{(1+s)\bar{r}\varphi_j}{2}\mathrm{d}s, \tag{C.8a}$$

$$\int_{(l_1-r)\varphi_j}^{(l_1+r)\varphi_j} K_{ij}(\theta,k)\mathrm{d}\theta = -2r\varphi_j \int_{-1}^{1} I_{-1}\left(\frac{1}{k}\left|\sin\left[\frac{(l_1+rs)\varphi_j}{2} + \frac{\theta_i}{2}\right]\right.\right. \left.\left.\sin\left[\frac{(l_1+rs)\varphi_j}{2} - \frac{\theta_i}{2}\right]\right|\right) \sin\frac{(1+s)r\pi}{2}\sin\frac{(1-s)r\pi}{2} \sin\left[(l_1+rs)\varphi_j\right]\mathrm{d}s, \tag{C.8b}$$

$$\int_{(l_2-\bar{r})\varphi_j}^{(l_2+\bar{r})\varphi_j} K_{ij}(\theta,k)\mathrm{d}\theta = 2\bar{r}\varphi_j \int_{-1}^{1} I_{-1}\left(\frac{1}{k}\left|\sin\left[\frac{(l_2+\bar{r}s)\varphi_j}{2} + \frac{\theta_i}{2}\right]\right.\right. \left.\left.\sin\left[\frac{(l_2+\bar{r}s)\varphi_j}{2} - \frac{\theta_i}{2}\right]\right|\right) \sin\frac{(1+s)\bar{r}\pi}{2}\sin\frac{(1-s)\bar{r}\pi}{2} \sin\left[(l_2+\bar{r}s)\varphi_j\right]\mathrm{d}s, \tag{C.8c}$$

$$\int_{\pi-r\varphi_j}^{\pi} K_{ij}(\theta,k)\mathrm{d}\theta = -r\varphi_j \int_{-1}^{1} I_{-1}\left(\frac{1}{k}\left|\cos\left[\frac{(1-s)r\varphi_j}{4} + \frac{\theta_i}{2}\right]\right.\right. \left.\left.\cos\left[\frac{(1-s)r\varphi_j}{4} - \frac{\theta_i}{2}\right]\right|\right) \sin\frac{(1+s)r\pi}{4} \sin\frac{(3-s)r\pi}{4}\sin\frac{(1-s)r\varphi_j}{2}\mathrm{d}s. \tag{C.8d}$$

The integrals given by Eqs. (C.7) and (C.8) are evaluated by using adaptive quadrature [47] with a specified absolute tolerance ϵ. In particular, we use the generalized Gaussian quadrature for products of a polynomial and logarithmic function [47]. The generalized Gaussian quadrature [47] with 40 abscissas and a tolerance $\epsilon = 10^{-15}$ can maintain the error in the integral in Eq. (4b) at $O(10^{-11})$ or smaller for $0.003 \leqslant k \leqslant 10.0$.

References

[1] Gross EP, Jackson EA, Ziering S. Boundary value problems in kinetic theory of gases. Ann Phys 1957;1:141–67.
[2] Williams MMR. A review of the rarefied gas dynamics theory associated with some classical problems in flow and heat transfer. Z Angew Math Phys 2001;52(3):500–16.
[3] Kogan MN. Rarefied gas dynamics. New York: Plenum Press; 1969.
[4] Cercignani C. The Boltzmann equation and its applications. New York: Springer; 1988.

[5] Cercignani C, Illner R, Pulvirenti M. The mathematical theory of dilute gases. New York: Springer; 1994.
[6] Cercignani C. Rarefied gas dynamics: from basic concepts to actual calculations. Cambridge, UK: Cambridge University Press; 2000.
[7] Ivchenko IN, Loyalka SK, Tompson Jr RV. Analytical methods for problems of molecular transport. Fluid mechanics and its applications, vol. 83. Dordrecht, The Netherlands: Springer; 2007.
[8] Sone Y. Molecular gas dynamics: theory, techniques, and applications. Boston: Birkhäuser; 2007.
[9] Gross EP, Jackson EA. Kinetic models and the linearized Boltzmann equation. Phys Fluids 1959;2(4):432–41.
[10] Willis DR. Comparison of kinetic theory analyses of linearized Couette flow. Phys Fluids 1962;5(2):127–35.
[11] Albertoni S, Cercignani C, Gotusso L. Numerical evaluation of the slip coefficient. Phys Fluids 1963;6(7):993–6.
[12] Cercignani C, Pagani CD. Variational approach to boundary-value problems in kinetic theory. Phys Fluids 1966;9(6):1167–73. http://dx.doi.org/10.1063/1.1761816.
[13] Cercignani C, Sernagiotto F. Cylindrical Couette flow of a rarefied gas. Phys Fluids 1967;10(6):1200–4. http://dx.doi.org/10.1063/1.1762263.
[14] Loyalka SK. Velocity profile in Knudsen layer for Kramer's problem. Phys Fluids 1975;18(12):1666–9.
[15] Loyalka SK. Some exact numerical results for the BGK model: Couette, Poiseuille and thermal creep flow between parallel plates. Z Angew Math Phys 1979;30(3):514–21.
[16] Coron F. Derivation of slip boundary-conditions for the Navier–Stokes system from the Boltzmann equation. J Stat Phys 1989;54(3/4):829–57. http://dx.doi.org/10.1007/BF01019777.
[17] Loyalka SK, Hickey KA. The Kramer's problem: velocity slip and defect for a hard sphere gas with arbitrary accommodation. Z Angew Math Phys 1990;41(2):245–53.
[18] Sone Y, Takata S, Ohwada T. Numerical analysis of the plane Couette flow of a rarefied gas on the basis of the linearized Boltzmann equation for hard-sphere molecules. Eur J Mech B/Fluids 1990;9(3):273–88.
[19] Sharipov F, Seleznev V. Data on internal rarefied gas flows. J Phys Chem Ref Data 1998;27(3):657–706.
[20] Barichello LB, Camargo M, Rodrigues P, Siewert CE. Unified solutions to classical flow problems based on the BGK model. Z Angew Math Phys 2001;52(3):517–34. http://dx.doi.org/10.1007/PL00001559.
[21] Cercignani C, Lampis M, Lorenzani S. Plane Poiseuille–Couette problem in micro-electro-mechanical systems applications with gas-rarefaction effects. Phys Fluids 2006;18(8):087102. http://dx.doi.org/10.1063/1.2335847.
[22] Loyalka SK, Tompson RV. The velocity slip problem: accurate solutions of the BGK model integral equation. Eur J Mech B/Fluids 2009;28(2):211–3.
[23] Sharipov F. Data on the velocity slip and temperature jump on a gas–solid interface. J Phys Chem Ref Data 2011;40(2):023101.
[24] Gibelli L. Velocity slip coefficients based on the hard-sphere Boltzmann equation. Phys Fluids 2012;24(2):022001. http://dx.doi.org/10.1063/1.3680873.
[25] Yap YW, Sader JE. High accuracy numerical solutions of the Boltzmann Bhatnagar–Gross–Krook equation for steady and oscillatory Couette flows. Phys Fluids 2012;24(3):032004.
[26] Kaneko H, Xu Y. Numerical solutions for weakly singular Fredholm integral equations of the 2nd kind. Appl Numer Math 1991;7(2):167–77.
[27] Kaneko H, Noren R. An application of approximation theory to numerical solutions for Fredholm integral equations of the 2nd kind. Numer Funct Anal Opt 1991;12(5–6):517–23. http://dx.doi.org/10.1080/01630569108816447.
[28] Tweed J, John RSt, Dunn MH. Algorithms for the numerical solution of a finite-part integral equation. Appl. Math. Lett. 1999;12(3):3–9. http://dx.doi.org/10.1016/S0893-9659(98)00163-3.
[29] Helsing J, Ojala R. Corner singularities for elliptic problems: integral equations, graded meshes, quadrature, and compressed inverse preconditioning. J Comput Phys 2008;227:8820–40.
[30] Bremer J, Gimbutas Z, Rokhlin V. A nonlinear optimization procedure for generalized Gaussian quadratures. SIAM J Sci Comput 2010;32:1761–88.
[31] Bremer J, Rokhlin V. Efficient discretization of Laplace boundary integral equations on polygonal domains. J Comput Phys 2010;229:2507–25.
[32] Bremer J, Rokhlin V, Sammis I. Universal quadratures for boundary integral equations on two-dimensional domains with corners. J Comput Phys 2010;229:8259–80.
[33] Helsing J. A fast and stable solver for singular integral equations on piecewise smooth curves. SIAM J Sci Comput 2011;33:153–74.
[34] Bremer J. A fast direct solver for the integral equations of scattering theory on planar curves with corners. J Comput Phys 2012;231:1879–99.
[35] Helsing J. Solving integral equations on piecewise smooth boundaries using the RCIP method: a tutorial. Abstr Appl Anal 2013;2013:938167.
[36] Atkinson KE. The numerical solution of integral equations of the second kind, cambridge monographs on applied and computational mathematics. Cambridge, UK: University of Cambridge Press; 1997.
[37] Mathai AM, Saxena RK. Generalized hypergeometric functions with applications in statistics and physical sciences. Berlin, Germany: Springer; 1973.
[38] Beals R, Szmigielski J. Meijer g-functions: a gentle introduction. Notices AMS 2013;60(7):866–72.
[39] MacLeod AJ. Private communications; 2013.
[40] Yap YW. Rarefied gas dynamics: stokes' second problem. Honours thesis, The University of Melbourne, Victoria, Australia; 2009.
[41] MacLeod AJ. Chebyshev expansion for Abramowitz functions. Appl Numer Math 1992;10:129–37.
[42] Maxwell JC. On stresses in rarified gases arising from inequalities of temperature. Philos Trans Roy Soc London 1879;170:231–56.
[43] Bhatnagar PL, Gross EP, Krook M. A model for collision processes in gases. I. Small amplitude processes in charged and neutral one-component systems. Phys Rev 1954;94(3):511–25.
[44] Sone Y. Kinetic theory analysis of linearized Rayleigh problem. J Phys Soc Jpn 1964;19(8):1463–73.
[45] Sone Y. Kinetic theory analysis of the linearized Rayleigh problem. Phys Fluids 1964;7(3):470–1. http://dx.doi.org/10.1063/1.1711221.
[46] Jiang S. Private communications; 2013.
[47] Ma J, Rokhlin V, Wandzura S. Generalized Gaussian quadrature rules for systems of arbitrary functions. SIAM J Numer Anal 1996;33(3):971–96.
[48] C++/Fortran-90 arbitrary precision package (ARPREC). <http://crd-legacy.lbl.gov/dhbailey/mpdist/>.
[49] Clenshaw CW. A note on the summation of Chebyshev series. Math Comput 1955;9:118–20.
[50] Einzel D, Panzer P, Liu M. Boundary condition for fluid flow: curved or rough surfaces. Phys Rev Lett 1990;64:2269–72. http://dx.doi.org/10.1103/PhysRevLett.64.2269.
[51] Lockerby DA, Reese JM, Emerson DR, Barber RW. Velocity boundary condition at solid walls in rarefied gas calculations. Phys Rev E 2004;70(1):017303. http://dx.doi.org/10.1103/PhysRevE.70.017303.
[52] O'Hare L, Lockerby DA, Reese JM, Emerson DR. Near-wall effects in rarefied gas micro-flows: some modern hydrodynamic approaches. Int J Heat Fluid Flow 2007;28(1):37–43. http://dx.doi.org/10.1016/j.ijheatfluidflow.2006.04.012.
[53] Cercignani C, Lorenzani S. Variational derivation of second-order slip coefficients on the basis of the Boltzmann equation for hard-sphere molecules. Phys Fluids 2010;22(6). http://dx.doi.org/10.1063/1.3435343.
[54] Zhang W-M, Meng G, Wei X. A review on slip models for gas microflows. Microfluid Nanofluid 2012;13(6):845–82. http://dx.doi.org/10.1007/s10404-012-1012-9.
[55] Guo ZL, Qin JH, Zheng CG. Generalized second-order slip boundary condition for nonequilibrium gas flows. Phys Rev E 2014;89:013021. http://dx.doi.org/10.1103/PhysRevE.89.013021.
[56] Lockerby DA, Reese JM, Gallis MA. The usefulness of higher-order constitutive relations for describing the Knudsen layer. Phys Fluids 2005;17(10):109902. http://dx.doi.org/10.1063/1.1897005.
[57] Loyalka SK. Thermal transpiration in a cylindrical tube. Phys Fluids 1969;12(11):2301–5. http://dx.doi.org/10.1063/1.1692346.
[58] Valougeorgis D, Thomas Jr JR. Exact numerical results for Poiseuille and thermal creep flow in a cylindrical tube. Phys Fluids 1986;29(2):423–9.
[59] Barichello LB, Camargo M, Rodrigues P, Siewert CE. An integral equation basic to the BGK model for flow in a cylindrical tube. Z Angew Math Phys 2002;53(5):769–81. http://dx.doi.org/10.1007/s00033-002-8182-3.
[60] Siewert CE. Poiseuille, thermal creep and Couette flow: Results based on the CES model of the linearized Boltzmann equation. Eur J Mech B/Fluids 2002;21(5):579–97. http://dx.doi.org/10.1016/S0997-7546(02)01202-5.
[61] Siewert CE. The linearized Boltzmann equation: concise and accurate solutions to basic flow problems. Z Angew Math Phys 2003;54(2):273–303. http://dx.doi.org/10.1007/s000330300005.
[62] Andallah LS, Babovsky H. A discrete Boltzmann equation based on hexagons. Math Models Methods Appl Sci 2003;13(11):1537–63.
[63] Andallah LS, Babovsky H. A discrete Boltzmann equation based on a cub-octahedron in $\mathbb{R}^3$. SIAM J Sci Comput 2008;31(2):799–825. http://dx.doi.org/10.1137/060673850.
[64] Xu K, Li Z. Microchannel flow in the slip regime: gas-kinetic BGK-Burnett solutions. J Fluid Mech 2004;513:87–110. http://dx.doi.org/10.1017/S0022112004009826.
[65] Guo ZL, Xu K, Wang R. Discrete unified gas kinetic scheme for all Knudsen number flows: low-speed isothermal case. Phys Rev E 2013;88(3):033305. http://dx.doi.org/10.1103/PhysRevE.88.033305.
[66] Abramowitz M, Stegun IA, editors. Handbook of mathematical functions with formulas, graphs, and mathematical tables. Washington, DC: National Bureau of Standards; 1964.